A NUMERICALLY STABLE MODEL FOR SIMULATING HIGH FREQUENCY CONDUCTION BLOCK IN NERVE FIBER

A Thesis
Presented to
The Academic Faculty

by

Rebecca Kieselbach

In Partial Fulfillment
of the Requirements for the Degree
Master of Science in the
School of Electrical and Computer Engineering

Georgia Institute of Technology
August 2011

A NUMERICALLY STABLE MODEL FOR SIMULATING HIGH FREQUENCY CONDUCTION BLOCK IN NERVE FIBER

Approved by:

Professor Robert Butera, Advisor
School of Electrical and Computer Engineering
Georgia Institute of Technology

Professor Pamela Bhatti
School of Electrical and Computer Engineering
Georgia Institute of Technology

Professor William Hunt
School of Electrical and Computer Engineering
Georgia Institute of Technology

Date Approved: May 18 2011

ACKNOWLEDGEMENTS

I want to thank my adviser, Dr. Robert Butera, for his guidance and support. I would also like to thank any others who have helped me in some way during this project, including the Butera lab group and my fiancé, Lester Li.

TABLE OF CONTENTS

ACKNOWLEDGEMENTS . . . . . **iii**

LIST OF FIGURES . . . . . **v**

SUMMARY . . . . . **vii**

I INTRODUCTION **1**

II BACKGROUND **2**

2.1 Experiments 2

2.2 Modeling 7

III METHODS **16**

3.1 Implementation of the unmodified cable model with extracellular stimulation 16

3.2 Modification of the cable model to include a frequency-dependent capacitance 19

3.2.1 Defining the relationship between frequency and membrane capacity 19

3.2.2 Incorporating the FDC in to the cable model 20

3.2.3 Approximating the modified cable model 22

3.2.4 Solving the modified cable model 28

IV RESULTS **30**

4.1 Unmodified cable model verification 30

4.2 Modified cable model verification 33

V CONCLUSION **39**

REFERENCES **40**

LIST OF FIGURES

1 Block diagram of the experimental set-up used to induce conduction block and measure muscle response. K.L. Kilgore and N. Bhadra (2006) 3

2 Monotonic response of voltage threshold needed to induce HFAC block in the pudendal nerve plotted as a function of frequency. Bhadra et al. (2006) . . 4

3 Schematic of the experimental setup used to induce and measure HFAC block in Aplysia nerve. Joseph and Butera (2009) 5

4 Nonmonotonic response of current threshold needed to induce HFAC block in Aplysia nerve. Joseph and Butera (2009) 6

5 Average current block threshold of A and C fibers of the sciatic nerve of rats. L. Joseph and R.J. Butera (2011) 6

6 Electrical schematic of the membrane of a squid axon. A. L. Hodgkin and A. F. Huxley (1952) 7

7 Diagram of current flow in cylindrical cable model. 10

8 Electrical schematic of passive cable model. 10

9 Electrical schematic of nonlinear cable model. The block represents the ion channels from the Hodgkin-Huxley model. 11

10 Diagram of current flow in cylindrical cable model with extracellular stimulation. 12

11 Electrical schematic of nonlinear cable model with external stimulation. The block represents the ion channels from the Hodgkin-Huxley model. 13

12 $\frac{\partial^2 V_e}{\partial x^2}$ and V_e resulting from a point source 1mm away from a 10mm fiber with anodal (1450μA) and cathodal (-290μA) current sources. The x-axis shows the length of the cable in mm. The y-axis shows the value of $\frac{\partial V_e}{\partial t}$ and V_e along the cable. Rattay (1986) 13

13 Diagram of the triggering and subsequent blocking of APs using extracellular stimulation. 14

14 Membrane capacitance of the giant squid axon as a function of stimulus frequency. The different data markers represent the different experimental setups that were used to obtain readings of the capacity. Haydon and Urban (1985). 15

15 Superposition of the external voltage on the cable determined by solving the Activating Function at each point. 16

16 Membrane capacity as a function of stimulus frequency. The data points are from Haydon and Urban (1983) and the line fitted to the data is described by Equation 30. 20

17 Threshold current as a function of the fiber diameter. Stimulation occurs from a rectangular cathodal impulse of 0.1 ms, 1 mm away from the axon. The axon parameters used are those of squid nerve fiber. 30

18 Plot of AP excitation as a function of electrode current and distance to the fiber. The model uses the squid axon properties and a fiber diameter of 9.6μm. 31

19 Relationship between block current threshold and fiber diameter for various frequencies. 32

20 Relationship between block current threshold and frequency for the unmodified cable model with and without clipping. The model is implemented with the parameters used in the comparison to Tai's paper. 33

21 Modified cable model without the FDC component. Membrane voltage and gating variable values as an action potential propagates through a node 1.75cm along a cable with a 10μm diameter. The AP was generated by applying a -3mA current pulse at 0.1ms from the simulation start and no blocking stimulus. 34

22 Relationship between block threshold and fiber diameter for various frequencies. 35

23 Membrane voltage and gating variable values as an action potential propagates through a node 1.75cm along a cable with a 10μm diameter. 35

24 The membrane capacitance in varied in a Hodgkin-Huxley model (resting potential = -65mV) with a rectangular pulse stimulus of amplitude 20μA applied at 5ms. 36

25 Relationship between block current threshold and frequency for the modified (FDC) and unmodified cable model. Stimuli are 0.1cm away from an axon with diameter = 10um and length = 4cm. 37

26 Relationship between block current threshold and frequency for the FDC model, as results from different time (dt) and space (dx) steps. 37

SUMMARY

Previous studies performed on myelinated nerve fibers have shown that a high frequency alternating current stimulus can block impulse conduction. The current threshold at which block occurs increases as the blocking frequency increases. Cable models based on the Hodgkin-Huxley model are consistent with these results.

Recent experimental studies on unmyelinated nerve have shown that at higher frequencies, the block threshold decreases. When the block threshold is plotted as a function of frequency the resulting graph is distinctly nonmonotonic. Currently, all published models do not explain this behavior and the physiological mechanisms that create it are unknown. This difference in myelinated vs. unmyelinated block thresholds at high frequencies could have numerous clinical applications, such as chronic pain management.

A large body of literature has shown that the specific capacitance of biological tissue decreases at frequencies in the kHz range or higher. Prior research has shown that introducing a frequency-dependent capacitance (FDC) to the Hodgkin-Huxley model will attenuate the block threshold at higher frequencies, but not to the extent that was seen in the experiments. This model was limited by the methods used to solve its higher order partial differential equation. The purpose of this thesis project is to develop a numerically stable method of incorporating the FDC into the model and to examine its effect on block threshold. The final, modified model will also be compared to the original model to ensure that the fundamental characteristics of action potential propagation remain unchanged.

CHAPTER I

INTRODUCTION

Clinical and modeling studies have shown that high-frequency alternating current (HFAC) stimulation can block conduction in nerves. The HFAC amplitude at which this block first occurs is referred to as the block threshold; it has been proven to increase as a function of the HFAC frequency [1], [2], [3], [17]. Laboratory experiments exploring this behavior have been performed using mixed myelinated and unmyelinated nerve fibers. It was later shown that, in purely unmyelinated nerve fiber, block threshold increased as a function of frequency up to a point before decreasing, resulting in a nonmonotonic response. By varying the frequency of the HFAC stimulus, it may be possible to selectively block different nerves. The ability to control the propagation of signals in the body has various clinical applications, including chronic pain management.

While this response has been observed clinically, computational studies could not replicate the nonmonotonic behavior; possibly because the axon models may not be completely accurate representations of unmyelinated nerve fiber. The foundation of these axon models, the Hodgkin-Huxley model, assumes a fixed membrane capacitance. However, experimental studies have shown that the membrane capacity changes as a function of stimulus frequency [8]. A model incorporating a frequency-dependent capacitance (FDC) caused the relationship between block threshold and frequency to closer resemble the nonmonotonic blocking response observed in clinical studies [7].

However, this model has limitations stemming from the methods used to solve its complex system of partial differential equations. This thesis will present a model incorporating the FDC, implemented using numerical methods that prove to be more stable and computationally time-efficient.

CHAPTER II

BACKGROUND

2.1 Experiments

Clinical studies have demonstrated that nerve fiber conduction can be blocked with the introduction of either alternating current (AC) or direct current (DC) stimuli. Researchers have utilized different methods and experimental setups to determine the mechanisms that enable blocking, however they are still not fully understood. The bulk of these studies have been conducted using a high frequency alternating current (HFAC) blocking stimulus on mammalian or amphibian nerve fibers.

A typical experimental setup involves isolating the nerve fiber from the animal and attaching electrodes to stimulate and measure compound action potential (CAP) propagation. The CAP is the sum of the extracellular electric field potential created by the electrical activity of a bundle of nerves in a fiber. A more functional preparation measures the twitch response of muscles connected to the nerve fiber to quantify the effect of HFAC block. Figure 1 shows this particular experimental set-up. An electrode is attached to the proximal nerve to generate an action potential and another electrode is placed between it and the muscle to produce conduction block stimulus [3].

The first group to attempt to isolate the cause of HFAC block was Cattel and Gerard (1935) [5]. They used a low frequency stimulus of 500-600Hz and a high of 2300Hz. Their research led them to conclude that a decrease in the excitability of the nerve fiber at the block site could block impulse propagation at that location. This assertion was supported by Reboul and Rosenblueth (1939) detailing the effects of HFAC stimulus of up to 40kHz on the feline popliteal nerve fiber [16].

Over twenty years later, Tanner (1962) briefly investigated reversible blocking in the sciatic nerve of large green frogs [18]. Through the application of a 20kHz blocking signal, he was able to observe that nerve fibers of varying diameters would react differently to a

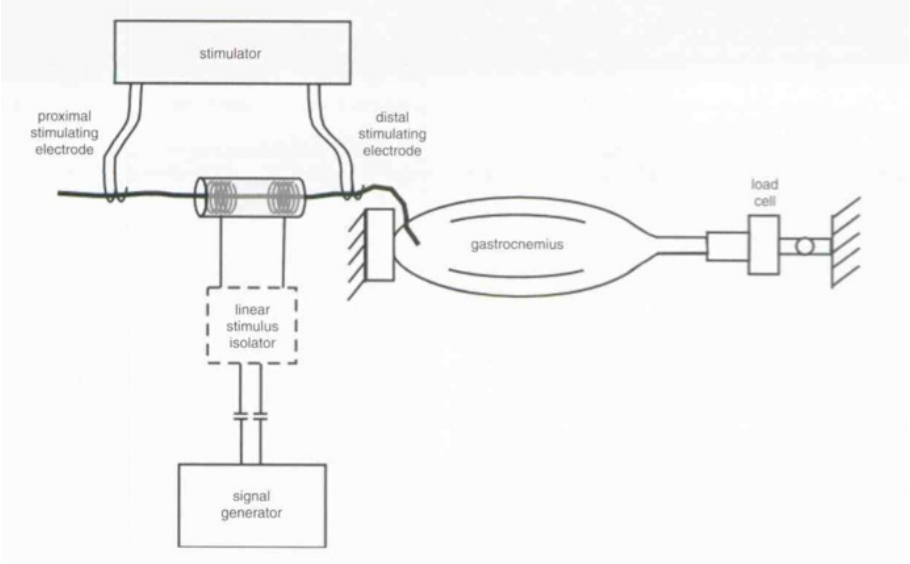

Figure 1: Block diagram of the experimental set-up used to induce conduction block and measure muscle response. K.L. Kilgore and N. Bhadra (2006)

given block amplitude. He noted that smaller fibers would experience larger currents and therefore a larger depolarizing effect.

Woo and Campbell (1964) examined the effect of HFAC block in the sciatic nerves of frogs and the tibial nerves of cats [19]. By varying the amplitude of a 20kHz blocking stimulus, they observed change in the neuron response. At low amplitudes, the nerve fiber exhibited rhythmic firing. As the amplitude of the blocking stimulus was increased, the firing frequency increased until it became sporadic passed 400-700Hz before stopping completely. After demonstrating blocking using HFAC stimuli, Woo and Campbell researched conduction block using DC blocking stimuli.

Bowman and McNeal (1986) experimented with a stimulus consisting of rectangular pulses ranging from 100 to 10,000Hz [4]. When applied to the sciatic nerves of cats, they observed that a block could be achieved at 4kHz with a blocking amplitude five times that of the threshold voltage. The high frequency stimulus initially generates 1-2 seconds of firing before blocking truly occurs, which is reversible around 1 second after the blocking stimulus is removed. Their experimentation revealed that there is a frequency threshold at which block occurs.

Kilgore and Bhadra (2005) found that a fully reversible conduction block could be achieved in the sciatic nerves of frogs using a 3-5kHz sinusoidal waveform with 0.5-2mA amplitude [2]. Both experimental results and computer modeling led them to conclude that conduction block is due to the depolarization of the nerve fiber around the block site.

HFAC block is not only reversible, as demonstrated in these papers, but also exhibits a particular response to changes in blocking amplitude. Bhadra et al. (2006) detailed the effect of conduction block on the pudendal nerves of cats [3]. They established that the threshold amplitude of the block stimulus voltage increases as a function of the frequency; Figure **??** shows the monotonic block threshold-frequency relationship.

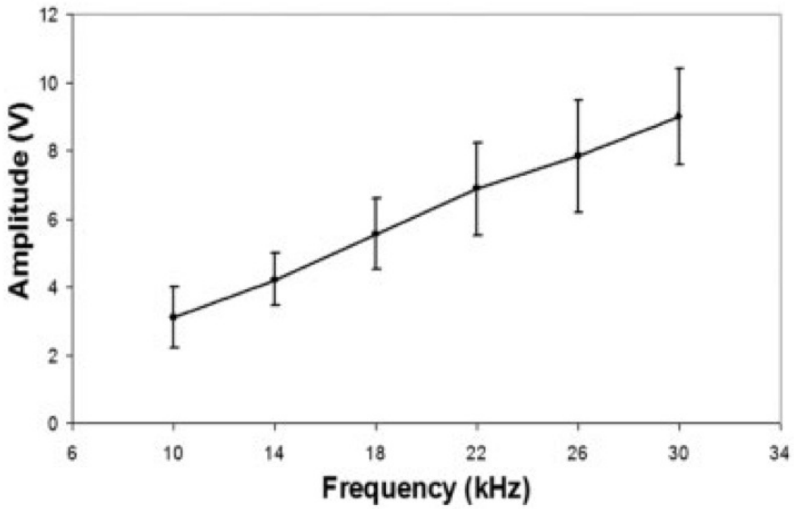

Figure 2: Monotonic response of voltage threshold needed to induce HFAC block in the pudendal nerve plotted as a function of frequency. Bhadra et al. (2006)

Many of these studies were conducted using mammalian or amphibian neurons, which contain myelinated nerve fibers. A more recent study, using purely unmyelinated Aplysia nerves, uncovered a significantly different blocking response. Joseph and Butera (2009) showed that a consistent, reversible conduction block could be achieved using HFAC stimulation [11]. Four suction electrodes were positioned along the fiber, as seen in Fig. 3.

One electrode initiated the action potential and another provided the HFAC block; the other two electrodes were used to record the propagation of the compound action potential. Sinusoidal or biphasic rectangular waveforms of 5-50kHz were used to induce block. At each

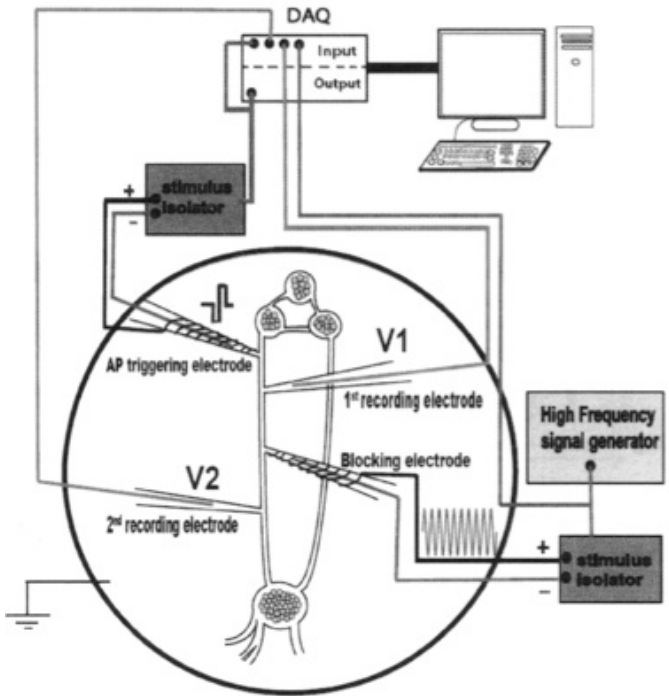

Figure 3: Schematic of the experimental setup used to induce and measure HFAC block in Aplysia nerve. Joseph and Butera (2009)

HFAC stimulus frequency, the current amplitude was varied until block occurred, producing a distinct relationship between frequency and current intensity threshold. As depicted in Figure 4, block amplitude increases as a function of frequency until 12kHz, at which point it decreases until the maximum test frequency is reached at 50kHz.

Unlike the previous experiments, which were conducted with a mix of myelinated and unmyelinated nerve fibers, the purely unmyelinated nerves demonstrate a nonmonotonic relationship between block threshold and frequency. To help explain this disparity, the experiment was repeated using the sciatic nerve of frogs, which are a mix of myelinated and unmyelinated fibers. The compound action potential was measured to determine if block had occurred; after which, the A and C components of the measurement were isolated to determine the individual effect of HFAC block. The A component is dominated by myelinated fibers, while the C component represents activity of a subset of unmyleinated fibers. It was possible to isolate the A and C fiber components because the C fiber has a slower conduction velocity and a distinct CAP shape, causing its response to appear 20ms

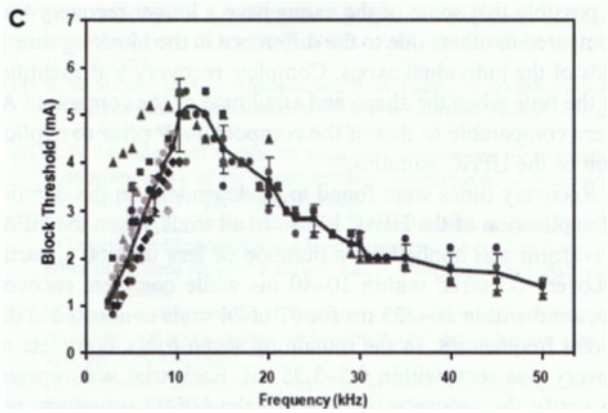

Figure 4: Nonmonotonic response of current threshold needed to induce HFAC block in Aplysia nerve. Joseph and Butera (2009)

after the A fiber response. The experiment was repeated using a range of frequencies from 5-50kHz on 9 nerves. The average block threshold of the A and C fibers versus frequency is shown in Fig. 5. Figure 5 shows that, at lower frequencies, there is a range of current amplitudes where A fiber is blocked, but C fiber is not [12]. While at higher frequencies, C fiber is blocked and A fiber is not.

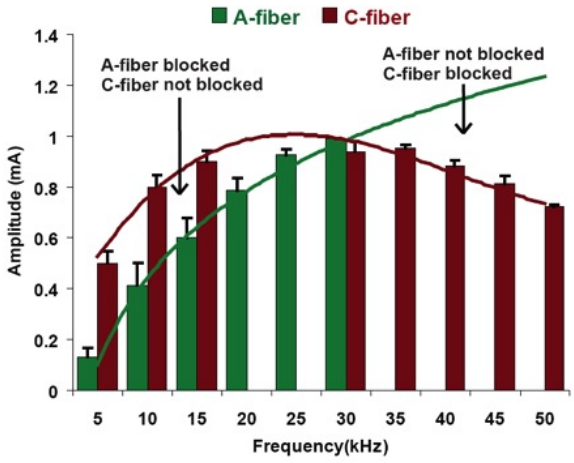

Figure 5: Average current block threshold of A and C fibers of the sciatic nerve of rats. L. Joseph and R.J. Butera (2011)

2.2 Modeling

Modeling is a useful tool in understanding the mechanisms that allow for nerve conduction and, more recently, conduction block. Modeling of the nerve began in 1952 when Hodgkin and Huxley [9] published a series of papers asserting that the electrical behavior of a unmyelinated giant squid axon could be represented by the electrical circuit in Fig. 6.

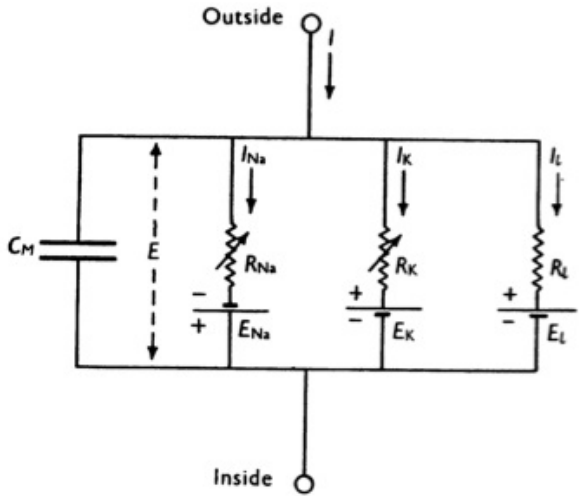

Figure 6: Electrical schematic of the membrane of a squid axon. A. L. Hodgkin and A. F. Huxley (1952)

Current flows through the membrane by charging the membrane capacitance or by the movement of ions through the ion channels, which are represented by parallel resistances. Current through the ion channels, called the ionic current, is comprised of potassium and sodium ions traveling through their respective channels. A leakage channel is also included to account for other ions such as chloride.

The ionic current densities (current per unit area) are determined by their individual ionic conductances (g_K for potassium, g_{Na} for sodium, and g_l for leakage) and Nernst potentials, which are the membrane potentials at which there is no net flow of the particular ions. Potassium and sodium channel conductances are nonlinear, being both voltage and time dependent. The leakage channel, however, contains a linear conductance. The individual current densities flowing through the ion channels are represented in Equations 1, 2,

and 3.

$$I_{Na}(V_m, t) = g_{Na}(V_m - E_{Na}), \tag{1}$$

$$I_K(V_m, t) = g_K(V_m - E_K), \tag{2}$$

$$I_l(V_m, t) = \bar{g}_l(V_m - E_l) \tag{3}$$

The ionic current density is the sum of the individual ion channel current densities, expressed in Eq. 4.

$$I_i = I_{Na} + I_K + I_l \tag{4}$$

The total current density through the membrane is a combination of the current through the membrane capacitance and the ionic current described previously. The capacitive current is a function of the membrane capacitance per unit area, which is assumed to be a fixed value, as well as the derivative of the membrane voltage (Eq. 5).

$$I = C_m \frac{\partial V_m}{\partial t} + I_i \tag{5}$$

To model the behavior of the ionic conductances, Hodgkin and Huxley fitted curves to experimental data of the changes in ionic conductances over time associated with the depolarization and repolarization of the nerve. The rise and fall of the ionic conductances caused by changes in membrane potential obey different first order equations. These equations solve for gating variables, which indicate how open a population of channels are. The potassium conductance can be modeled as being proportional to a variable to the fourth power (Eq. 6), where the variable is described by a first-order equation (Eq.74).

$$g_K = \bar{g_K} n^4 \tag{6}$$

$$\frac{\partial n}{\partial t} = \alpha_n(1 - n) - \beta_n n \tag{7}$$

α_n and β_n are rate constants dependent solely on voltage and n is a dimensionless variable with the range of zero to one. By solving Eq. 74 when the membrane potential is at rest, Hodgkin and Huxley were able to describe the rate constants as functions of the time constant, τ_n. In conjunction with the resting values of α_n and β_n, which were

obtained from fitting experimental data, Hodgkin and Huxley derived equations describing the potassium rate constants (Equations 8 and 9).

$$\alpha_n = 0.01(V + 10)/[exp(\frac{V + 10}{10}) - 1] \tag{8}$$

$$\beta_n = 0.125exp(V/80) \tag{9}$$

The sodium conductance equations were determined in a similar manner. However, the sodium conductance was found to be proportional to two variables both obeying first-order equations (Eq.'s 10, 11, and 12).

$$g_{Na} = \bar{g_K} m^3 h \tag{10}$$

$$\frac{\partial m}{\partial t} = \alpha_m(1 - m) - \beta_m m, \tag{11}$$

$$\frac{\partial h}{\partial t} = \alpha_h(1 - h) - \beta_h h \tag{12}$$

where,

$$\alpha_m = 0.1(V + 25)/[exp(\frac{V + 25}{10}) - 1] \tag{13}$$

$$\beta_m = 4exp(V/18), \tag{14}$$

$$\alpha_h = 0.07exp(V/20) \tag{15}$$

$$\beta_h = 1/[exp(\frac{V + 30}{10}) + 1] \tag{16}$$

Using these equations, Hodgkin and Huxley were able to model the electrical behavior of a single point on a nerve fiber.

The potential generated by an injected current flowing through the membrane may be great enough activate the voltage-gated ion channels. If the channels open, sodium ions will flow inward, causing the membrane potential to further increase, which in turn opens more sodium channels and the depolarization continues. At the peak of the action potential, the sodium channels close and the potassium channels dominate. The outward flow of potassium ions eventually causes the membrane potential to return to rest. The surge in membrane current caused by the ion channels is significantly larger than that of the stimulating current.

However, nerves come in many shapes and sizes and it is often necessary to have a model that can account for more than one point on the nerve. From this necessity, the cable model was developed using the simple geometry of a cylinder to represent the axon or sections of the dendrites. The cable model describes the flow of current through and along the membrane by segmenting the membrane so that the voltage and current can be calculated at each point (Fig. 7).

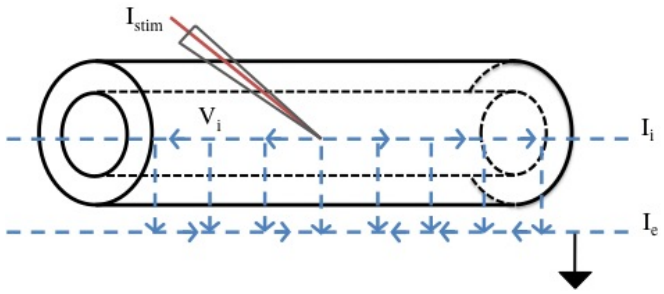

Figure 7: Diagram of current flow in cylindrical cable model.

In the passive cable model, each point along the cable length is approximated with a transmembrane capacitance and resistance, which are connected to each other with resistances approximating the internal and external resistance along membrane (Fig. 8).

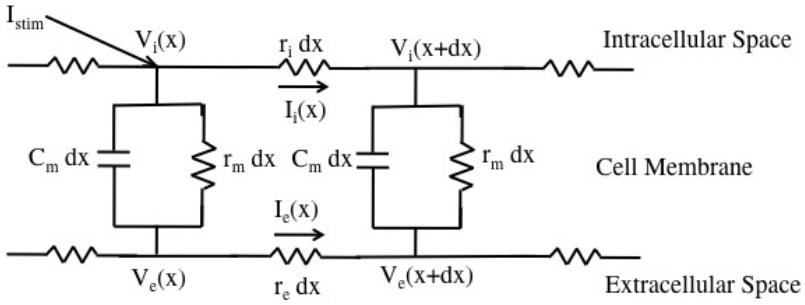

Figure 8: Electrical schematic of passive cable model.

According to Kirchoff's current laws, current that is introduced to the system will flow across and along the membrane; however, since this model lacks ion channels, no action potential will be generated from a stimulating current. To create a model with nonlinear properties, one that will generate and propagate action potentials, Hodgkin and Huxley's ion channel model will replace the fixed transmembrane resistance (Fig. 9).

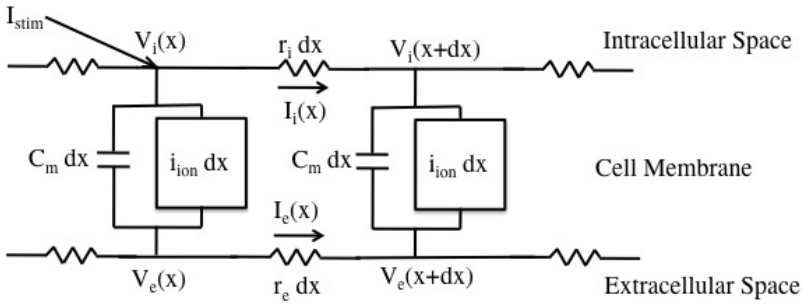

Figure 9: Electrical schematic of nonlinear cable model. The block represents the ion channels from the Hodgkin-Huxley model.

Unlike the Hodgkin-Huxley model, the cable model accounts for both the spatial as well as the temporal spread of potential. The membrane properties (resistances, capacitances, etc.) and the densities of the currents and voltages will have to be in terms of the cylinder's dimensions.

Using Kirchoff's current and voltage laws, expressions for the transmembrane current can be derived in terms of the membrane voltage and the injected current. One equation utilizes the derivative of the voltage with respect to the spacial dimension, x, and the other with respect to time, t. Set equal to each other, an equation is created describing the membrane voltage along an axon in terms of time and space (Eq. 17).

$$\frac{\partial V_m}{\partial t} = \frac{1}{4\pi(R_i + R_e)C_m}\frac{\partial^2 V_m}{\partial x^2} - \frac{V_m}{R_m C_m} + \frac{I_{inj}}{2\pi a C_m} \tag{17}$$

where,

- R_m is the transmembrane resistance in units of kohm cm
- R_i is the internal membrane resistance in units of kohm cm
- R_e is the external membrane resistance in units of kohm cm
- C_m is the membrane capacitance per unit area (μF/cm^2)
- a is the radius of the cylinder in cm
- V_m is the membrane voltage in mV

- I_{inj} is the injected current μA
- t is time in msec
- x is space in cm

In this model, current is injected directly into the membrane to generate an action potential (AP). However, it is possible to trigger an AP through external stimulation only. In this scenario, an electrode is placed within a few millimeters of the axon, where it generates an electro-magnetic field. This stimulus is modeled as a point current source lying in a uniform medium with the unmyelinated nerve fiber (Fig. 10). NcNeal (1976) assumed that the extracellular potential along the membrane would be fixed by the monopole's field [13]. It is then possible to calculate the potential at each node along the fiber (Φ_e) based on the distance to the point source (r), conductivity of the extracellular medium(σ_e), and the strength of the stimulating current (I_{stim})(Eq. 18).

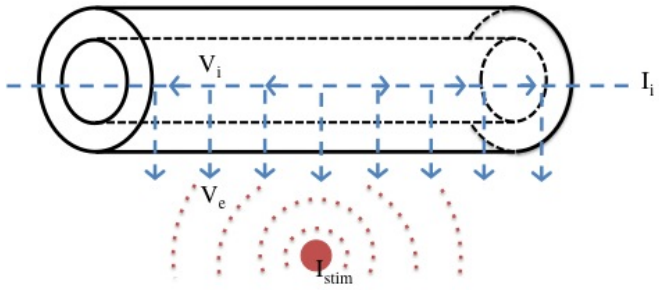

Figure 10: Diagram of current flow in cylindrical cable model with extracellular stimulation.

$$\Phi_e = \frac{I_{stim}}{4\pi\sigma_e r} \tag{18}$$

Since the extracellular membrane potential is fixed, there is no longer any current flowing along the outside of the membrane. The cable model is modified in Figure 11 to reflect this change.

When the cable equation is rederived based on this new model, it loses the extracellular resistance (r_e) and gains a term including the second derivative of extracellular membrane potential (Φ_e or V_e) with respect to space (Eq. 19). The derivative of the extracellular

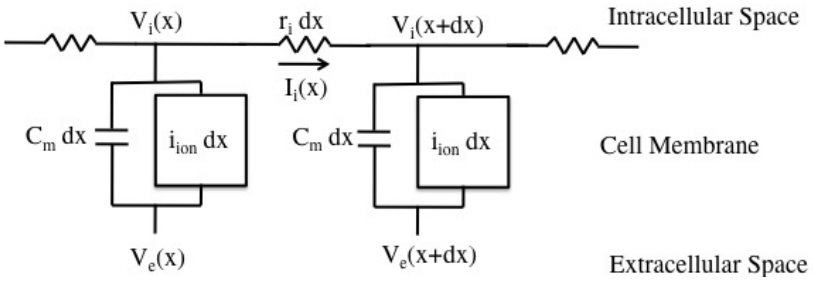

Figure 11: Electrical schematic of nonlinear cable model with external stimulation. The block represents the ion channels from the Hodgkin-Huxley model.

voltage can still be calculated independently of the cable equation as shown in Equation 20.

$$\frac{\partial V_m}{\partial t} = \frac{1}{C_m}\left[\frac{d}{4R_i}\frac{\partial^2 V_m}{\partial x^2} + \frac{d}{4R_i}\frac{\partial^2 V_e}{\partial x^2} - I_{ion}\right] \tag{19}$$

$$\frac{\partial^2 V_e}{\partial x^2} = \frac{I_{stim}}{4\pi\sigma_e}\left[\frac{2x^2 - h^2}{(h^2 + x^2)^{5/2}}\right] \tag{20}$$

Equation 20 is called the activating function because activation is only possible when $\frac{\partial V_m}{\partial t} > 0$, which Rattay assumed would occur when $\frac{\partial^2 V_e}{\partial x^2} > 0$ [14]. To illustrate the effect of the activating function, Rattay created a figure showing its behavior given a cathodal current source of -290μA and an anodal current of 1450μA (Fig. 12).

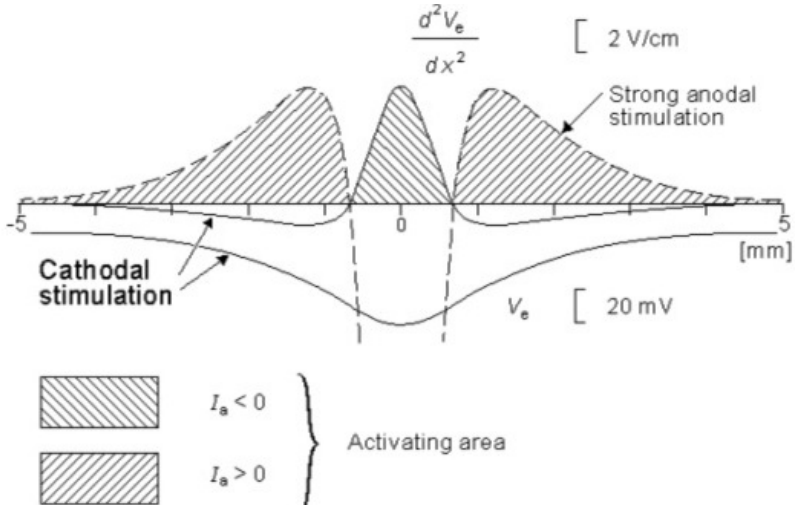

Figure 12: $\frac{\partial^2 V_e}{\partial x^2}$ and V_e resulting from a point source 1mm away from a 10mm fiber with anodal (1450μA) and cathodal (-290μA) current sources. The x-axis shows the length of the cable in mm. The y-axis shows the value of $\frac{\partial V_e}{\partial t}$ and V_e along the cable. Rattay (1986)

A strong anodal stimulus will cause $\frac{\partial^2 V_e}{\partial x^2}$ at the stimulus site (x=0 in Fig. 12) to be

very negative, making it difficult or even impossible to have an action potential occur there. However, on either side of the stimulus site, $\frac{\partial^2 V_e}{\partial x^2}$ becomes more positive, which could trigger APs. Cathodal stimulation does the opposite of an anodal source, but in a smaller scale. A slightly smaller negative current causes $\frac{\partial^2 V_e}{\partial x^2}$ to be positive at the stimulus site, possibly triggering APs. On either side of the site, $\frac{\partial^2 V_e}{\partial x^2}$ becomes negative and, if large enough, could prevent the propagation of APs.

This behavior can be used to both generate action potentials and block their propagation. Frequently in modeling studies of this effect, two extracellular sources are used: one to generate an AP with a rectangular pulse of current and the other to block the AP using a HFAC source (Fig. 13).

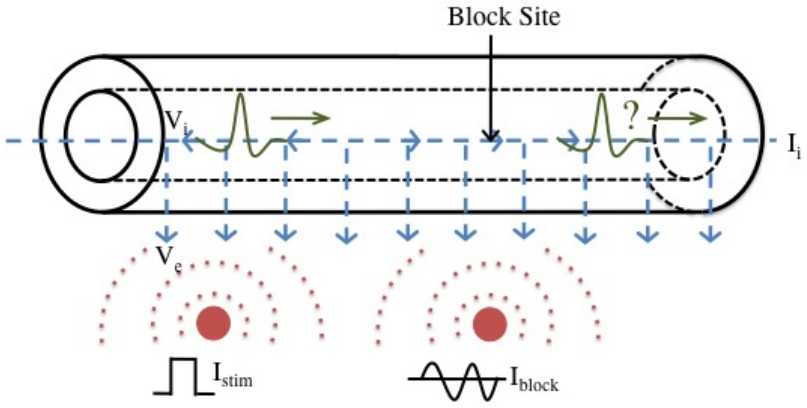

Figure 13: Diagram of the triggering and subsequent blocking of APs using extracellular stimulation.

Haeffele and Butera (2007) modified the cable model to determine the cause of the nonmonotonic blocking response seen in clinical studies of Aplysia nerves [7]. They incorporated a frequency-dependent capacitance in place of the fixed membrane capacitance in the Hodgkin-Huxley model. The evidence that the capacitance of unmyelinated nerve fiber is frequency-dependent came from Haydon and Urban's (1985) study of the giant squid axon under HFAC stimulation [8]. The membrane capacity was measured at different stimulus frequencies, the results are shown in Figure 14.

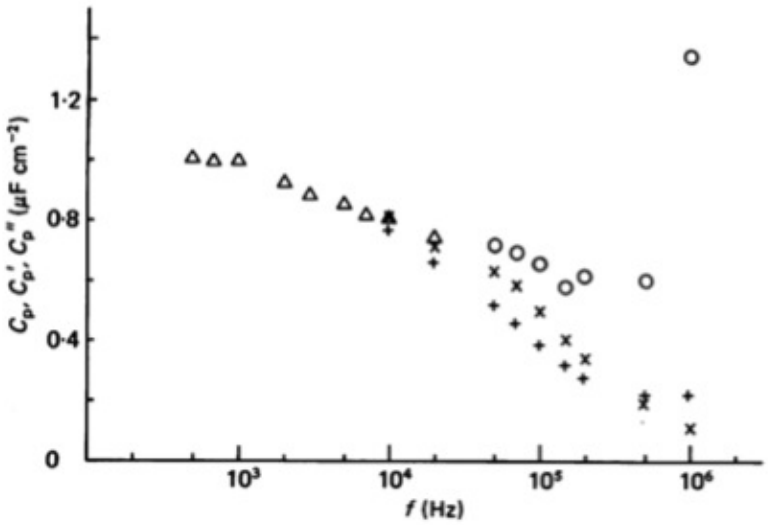

Figure 14: Membrane capacitance of the giant squid axon as a function of stimulus frequency. The different data markers represent the different experimental setups that were used to obtain readings of the capacity. Haydon and Urban (1985).

CHAPTER III

METHODS

3.1 Implementation of the unmodified cable model with extracellular stimulation

The purpose of first implementing the unmodified cable model is to establish a starting point with verifiable results for the new model. The cable model also provides a point of comparison for the modified model. As introduced in the Background, the cable model with extracellular stimulation is described by the following equation (Eq. 21).

$$\frac{\partial V_m}{\partial t} = \frac{1}{C_m}\left[\frac{1}{2\pi a r_i}\frac{\partial^2 V_m}{\partial x^2} + \frac{1}{2\pi a r_i}\frac{\partial^2 V_e}{\partial x^2} - I_{ion}\right] \tag{21}$$

$\frac{\partial^2 V_e}{\partial x^2}$ is solved analytically because it depends only on known quantities: the current amplitude, conductivity of the medium, and the position of the stimulus in relation to the fiber (Eq. 22).

$$\frac{\partial^2 V_e}{\partial x^2} = \frac{I_{stim}}{4\pi\sigma_e}\left[\frac{2x^2 - h^2}{(h^2 + x^2)^{5/2}}\right] \tag{22}$$

Before the system equations are solved, $\frac{\partial^2 V_e}{\partial x^2}$ is calculated at every point along the cable at every point in time. Figure 15 shows the superposition of V_e along the cable.

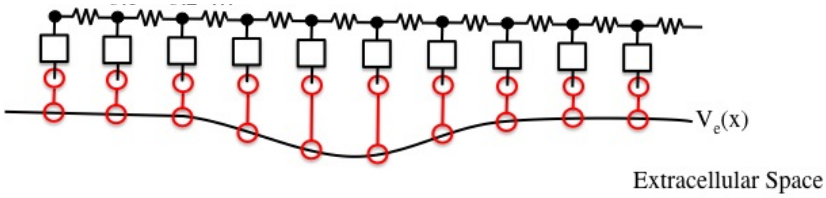

Figure 15: Superposition of the external voltage on the cable determined by solving the Activating Function at each point.

It is not possible to solve the cable equations analytically because they contain several higher order spacial and temporal derivatives,. Instead, the finite difference method will be used to approximate the system equations. A differential equation is numerically solved using algorithms and a set of initial conditions. The first step in this process is to discretize

the continuous system; the dimensions that exist in the system (space, time, etc.) must be broken down in to finite steps in time and space. These algorithms replace the derivative with approximately equivalent difference quotients, which use the distance between points and their values to estimate the next point. This model uses the backwards difference algorithms to approximate the temporal derivatives because this method requires only the solutions at previous time points. It is possible to estimate a partial differential equation as a system of linear ordinary differential equations, which can then be approximated using numerical methods. However, this approximation of the nonlinear PDE, coupled with ODEs, lends itself to errors.

The derivatives of the membrane voltage with respect to time and space are approximated in Equations 23 and 24. The temporal and spacial steps are represented by $\triangle t$ and $\triangle x$ respectively. The membrane voltage, V_m, will now be referred to by V.

$$\frac{\partial V_m}{\partial t} \approx \frac{V_t^x - V_{t-1}^x}{\triangle t} \tag{23}$$

$$\frac{\partial^2 V_m}{\partial x^2} \approx \frac{V_t^{x+1} - 2V_t^x + V_t^{x-1}}{\triangle x^2} \tag{24}$$

Substituting derivatives with their approximations results in Equation 25.

$$C_m \frac{V_t^x - V_{t-1}^x}{\triangle t} = \frac{1}{2\pi a r_i}\left[\frac{V_t^{x+1} - 2V_t^x + V_t^{x-1}}{\triangle x^2}\right] + \frac{1}{2\pi a r_i}\frac{\partial^2 V_e}{\partial x^2} - I_{ion} \tag{25}$$

The coefficients from Equation 25 are reorganized and new terms (Eq.'s 27 - 29) are defined. Equation 26 is then rewritten in matrix-vector form.

$$-\alpha V_t^{x+1} + (1+2\alpha)V_t^x - \alpha V_t^{x-1} = V_{t-1}^x + c\frac{\partial^2 V_e}{\partial x^2} - bI_{ion} \tag{26}$$

$$\alpha = \frac{\triangle t}{2\pi a r_i \triangle x^2 C_m} \tag{27}$$

$$b = \frac{\triangle t}{C_m} \tag{28}$$

$$c = \frac{\triangle t}{C_m 2\pi a r_i} \tag{29}$$

$$\begin{bmatrix} 1+\alpha & -\alpha & 0 & \dots & 0 \\ -\alpha & 1+2\alpha & \ddots & \dots & \vdots \\ 0 & \ddots & \ddots & -\alpha & 0 \\ \vdots & \dots & -\alpha & 1+2\alpha & -\alpha \\ 0 & \dots & 0 & -\alpha & 1+\alpha \end{bmatrix} \begin{bmatrix} V_t^1 \\ V_t^2 \\ V_t^3 \\ \vdots \\ V_t^n \end{bmatrix} = \begin{bmatrix} V_{t-1}^1 \\ V_{t-1}^2 \\ V_{t-1}^3 \\ \vdots \\ V_{t-1}^n \end{bmatrix} + c\frac{\partial^2 V_e}{\partial x^2} - bI_{ion}$$

In particular, the equation takes on the Ax=b form, where A is the symmetric, tridiagonal matrix, x is the unknown membrane voltage, and b is everything on the right-hand side of the equals sign. To solve this system, b must first be determined using the previous membrane voltage to calculate the ionic current from the Hodgkin-Huxley equations. The membrane voltage can then be solved for using the tridiagonal matrix algorithm. This voltage is used to recalculate the ionic currents and the process repeats itself until the membrane voltage has been solved for at each time point.

One important consideration in approximating the model's differential equations is numerical stability. A numerically stable algorithm has either no errors or no errors that grow rapidly during the calculations. Numerical stability is difficult to define when dealing with non-linear partial differential equations, such as the cable model, because they lack many of the well-defined characteristics of linear equations. Numerical stability can be effected by the number of significant digits used in the calculations; too few digits will result in large, uncontrollable errors. Therefore, the computational model is implemented using double precision numbers, which at 64 bits, are the largest format available in the C programming language.

Discrete equations will behave differently than the original differential equations because they are subject to the constraints of the temporal and spacial steps. At certain points along the cable, the membrane voltage will experience rapid changes in magnitude. This is most evident at the point where block occurs on the cable. This point is largely governed by the second derivative of the external voltage, which is determined by the high frequency stimulus. If the cable is not sampled at small enough intervals, the difference in voltage between the points becomes very large. This effect translates to the approximation

algorithms, where the error in the voltage estimates increase. The solution begins to blow up, eventually resulting in a mathematical singularity. To prevent this discontinuity, step sizes must be chosen carefully.

Another consideration in creating a numerically stable system is how to solve for the unknown x (the next V_m) from the Ax=b formulation. One method for solving this system is to represent it as a system of ordinary differential equations (ODEs) for each segment of time. Then, an ODE solver can be used to solve for x. However, this method is prone to error and instability. Another, more straightforward, method for solving this system is to multiply b and the inverse of A. Although this algorithm is computationally simple, and therefore faster, it is very likely to produce numerically unstable results. The tridiagonal matrix algorithm (TDMA) uses backward substitution to calculate the value of x, making the method backward stable. As a backward stable algorithm, the TDMA will help minimize errors in the solution, however it is more computationally expensive [6].

3.2 Modification of the cable model to include a frequency-dependent capacitance

The derivation of the modified cable model is split up into four major subsections:

- 3.2.1: Defining the relationship between frequency and membrane capacity
- 3.2.2: Incorporating the FDC in to the cable model
- 3.2.3: Approximating the modified cable model
- 3.2.4: Solving the modified cable model

3.2.1 Defining the relationship between frequency and membrane capacity

Haydon and Urban [8] showed that the membrane capacity decreases with increasing stimulating frequency. These frequencies are above the typical electrophysiological range, but within the firing range of the HFAC stimulus. Therefore, the capacity can no longer be

represented as a fixed quantity and must be described by a function of frequency. This function is fitted to the data from Haydon and Urban's 1983 paper using Matlab's Curve Fitting toolbox. While it is possible to fit many different types of functions to the data, it is crucial to consider how this function will be incorporated into the cable equation.

A function with a rational polynomial form allows for the most flexibility in fitting the data, providing multiple terms of varying degrees. Importantly, it is possible to take the Laplace transform of a polynomial expression, shifting it in to the same domain as the cable model equations. Figure 16 shows the frequency-dependent function (Eq. 30) plotted with the data points from Haydon and Urban. The equation is fitted upto 50kHz; anything larger is above the electrophysiological range.

$$C_m(s) = \frac{s^2 + 1.75 \cdot 10^5 s + 3.75 \cdot 10^9}{187.5 s^2 + 2.25 \cdot 10^7 s + 3.75 \cdot 10^{11}} \tag{30}$$

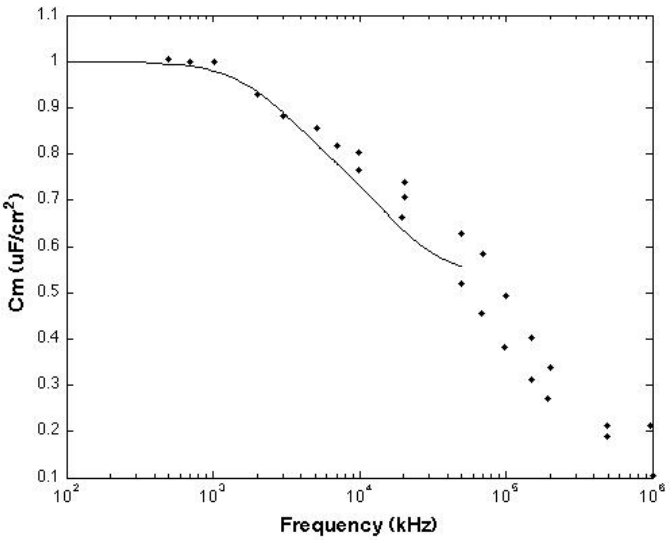

Figure 16: Membrane capacity as a function of stimulus frequency. The data points are from Haydon and Urban (1983) and the line fitted to the data is described by Equation 30.

3.2.2 Incorporating the FDC in to the cable model

As discussed previously, the frequency-dependent membrane capacitance can be expressed by a fitted rational polynomial. However, for the duration of this derivation, the symbolic

coefficients in Equation 31 will be used in place of these known quantities.

$$C_m(s) = \frac{b_0 s^2 + b_1 s + b_2}{a_1 s^2 + a_2 s + a_3} \tag{31}$$

The membrane capacitance can be expressed by the transfer function in Equation 32, where the ratio of the membrane voltage and capacitive current is equal to the electrical impedance of the capacity.

$$\frac{V_m(s)}{I_c(s)} = \frac{1}{sC_m(s)} \tag{32}$$

When the capacity transfer function (Eq. 31) is substituted into Equation 32, the transfer function can be rewritten as a function of the Laplace transforms of the membrane voltage and capacitive current only (Eq. 34). The inverse Laplace transform of Equation 34 is performed to move the equation into the time domain. The initial conditions of $V_m(s)$ and $I_C(s)$ and their derivatives are assumed to be equal to zero, resulting in Equation 35.

$$sV_m(s) = \frac{I_C(s)}{C_m(s)} = I_C(s)\left(\frac{a_1 s^2 + a_2 s + a_3}{b_0 s^2 + b_1 s + b_2}\right) \tag{33}$$

$$(b_0 s^3 + b_1 s^2 + b_2 s)V_m(s) = (a_1 s^2 + a_2 s + a_3)I_C(s) \tag{34}$$

$$b_0 \dddot{V_m} + b_1 \ddot{V_m} + b_2 \dot{V_m} = a_1 \ddot{I_C} + a_2 \dot{I_C} + a_3 I_C \tag{35}$$

The capacitive current is a function of the the extracellular voltage and the ionic current, which are only dependent on known quantities and the membrane voltage (Equation 36). In solving the model, I_C is calculated first, then used to solve for V_m in Equation 36. The new V_m is used to determine the next I_C and the process repeats itself.

$$I_C = C_m \frac{\partial V_m}{\partial t} = \frac{d}{4R_i}\left[\frac{\partial^2 V_m}{\partial x^2} + \frac{\partial^2 V_e}{\partial x^2}\right] - I_{ion} \tag{36}$$

Since we are dealing with a large system of differential equations, including a third-order differential equation, an analytical solution is not possible. However, the derivatives can be estimated using finite difference approximations. This method requires that the model be discretized; therefore, the cable space is broken into segments, $\triangle x$, and the time into $\triangle t$'s. Each side of Equation 35 is first approximated separately and then combined and transformed into a solvable matrix-vector system.

3.2.3 Approximating the modified cable model

3.2.3.1 Approximate $b_0\dddot{V}_m + b_1\ddot{V}_m + b_2\dot{V}_m$

The derivatives of V_m with respect to time are approximated using the backwards difference method. From this point on, the membrane potential, previously referred to as V_m, will be written as V.

$$b_0\dddot{V}_m + b_1\ddot{V}_m + b_2\dot{V}_m \approx b_0\frac{5V_t^x-18V_{t-1}^x+24V_{t-2}^x-14V_{t-3}^x+3V_{t-4}^x}{2\triangle t^3} + ... \\ b_1\frac{2V_t^x-5V_{t-1}^x+4V_{t-2}^x-V_{t-3}^x}{\triangle t^2} + b_2\frac{3V_t^x-4V_{t-1}^x+V_{t-2}^x}{2\triangle t} \tag{37}$$

The coefficients are grouped and assigned to new terms (Eq.'s 38-41) to minimize clutter in the final approximation.

$$V_t^x\left(\frac{5b_0}{2\triangle t^3}+\frac{2b_1}{\triangle t^2}+\frac{3b_2}{2\triangle t}\right)+V_{t-1}^x\left(\frac{-18b_0}{2\triangle t^3}-\frac{5b_1}{\triangle t^2}-\frac{4b_2}{2\triangle t}\right)+... \\ V_{t-2}^x\left(\frac{24b_0}{2\triangle t^3}+\frac{4b_1}{\triangle t^2}+\frac{b_2}{2\triangle t}\right)+V_{t-3}^x\left(\frac{-14b_0}{2\triangle t^3}-\frac{b_1}{\triangle t^2}\right)+V_{t-4}^x\left(\frac{3b_0}{2\triangle t^3}\right)$$

$$c_1 = \frac{5b_0}{2\triangle t^3}+\frac{2b_1}{\triangle t^2}+\frac{3b_2}{2\triangle t} = \frac{(5/2)b_0+2b_1\triangle t+(3/2)b_2\triangle t^2}{\triangle t^3} \tag{38}$$

$$c_2 = \frac{-18b_0}{2\triangle t^3}-\frac{5b_1}{\triangle t^2}-\frac{4b_2}{2\triangle t} = \frac{-9b_0-5b_1\triangle t-2b_2\triangle t^2}{\triangle t^3} \tag{39}$$

$$c_3 = \frac{24b_0}{2\triangle t^3}+\frac{4b_1}{\triangle t^2}+\frac{b_2}{2\triangle t} = \frac{12b_0+4b_1\triangle t+(1/2)b_2\triangle t^2}{\triangle t^3} \tag{40}$$

$$c_4 = \frac{-14b_0}{2\triangle t^3}-\frac{b_1}{\triangle t^2} = \frac{-7b_0-b_1\triangle t}{\triangle t^3} \tag{41}$$

$$c_5 = \frac{3b_0}{2\triangle t^3} \tag{42}$$

The resulting approximation (Eq. 43) will require three previous time steps to estimate the next membrane voltage, V_t^x.

$$b_0\dddot{V}_m + b_1\ddot{V}_m + b_2\dot{V}_m \approx c_1V_t^x + c_2V_{t-1}^x + c_3V_{t-2}^x + c_4V_{t-3}^x + c_5V_{t-4}^x \tag{43}$$

3.2.3.2 Approximate $a_1\ddot{I}_C + a_2\dot{I}_C + a_3I_C$

The membrane capacity current is determined from the cable equation with external stimulation (Eq. 44). Since I_{ion} and $\frac{\partial^2 V_e}{\partial x^2}$, are determined prior to the new V_m calculations,

they are isolated from the $\frac{\partial^2 V_m}{\partial x^2}$ term and assigned to a new term, γ. The calculation of γ is dealt with separately from this approximation. The membrane capacity current, which has been written as I_C, will now be referred to by I.

$$I_C = \frac{d}{4R_i}\left[\frac{\partial^2 V_m}{\partial x^2} + \frac{\partial^2 V_e}{\partial x^2}\right] - I_{ion} \tag{44}$$

$$= \frac{d}{4R_i}\frac{\partial^2 V_m}{\partial x^2} + \frac{d}{4R_i}\frac{\partial^2 V_e}{\partial x^2} - I_{ion} \tag{45}$$

$$= \omega\frac{\partial^2 V_m}{\partial x^2} + \gamma_t^x \tag{46}$$

where,

$$\omega = \frac{d}{4R_i} \tag{47}$$

$$\gamma_t^x = \frac{d}{4R_i}\frac{\partial^2 V_e(x,t)}{\partial x^2} - I_{ion}(x,t) \tag{48}$$

Since I_C contains a second-order spacial derivative, $\frac{\partial^2 V_e}{\partial x^2}$ must first be approximated before the time derivative approximations are determined (Eq. 49).

$$I_C = \omega\frac{\partial^2 V_m}{\partial x^2} + \gamma_t^x \approx \omega\left[\frac{V_t^{x+1} - 2V_t^x + V_t^{x-1}}{\triangle x^2}\right] + \gamma_t^x \tag{49}$$

The first and second time derivatives of I_C are determined using the backwards difference approximation method, as Equations 50 and 51 show.

$$\dot{I_C} \approx \frac{3I_t^x - 4I_{t-1}^x + I_{t-2}^x}{2\triangle t}$$
$$= \frac{3\omega\left[\frac{V_t^{x+1}-2V_t^x+V_t^{x-1}}{\triangle x^2}\right] + 3\gamma_t^x}{2\triangle t} + \frac{-4\omega\left[\frac{V_{t-1}^{x+1}-2V_{t-1}^x+V_{t-1}^{x-1}}{\triangle x^2}\right] - 4\gamma_{t-1}^x}{2\triangle t} + ...$$
$$\frac{\omega\left[\frac{V_{t-2}^{x+1}-2V_{t-2}^x+V_{t-2}^{x-1}}{\triangle x^2}\right] + \gamma_{t-2}^x}{2\triangle t} \tag{50}$$

$$\ddot{I_C} \approx \frac{2I_t^x - 5I_{t-1}^x + 4I_{t-2}^x - I_{t-3}^x}{\triangle t^2}$$
$$= \frac{2\omega\left[\frac{V_t^{x+1}-2V_t^x+V_t^{x-1}}{\triangle x^2}\right] + 2\gamma_t^x}{\triangle t^2} + \frac{-5\omega\left[\frac{V_{t-1}^{x+1}-2V_{t-1}^x+V_{t-1}^{x-1}}{\triangle x^2}\right] - 5\gamma_{t-1}^x}{\triangle t^2} + ...$$
$$\frac{4\omega\left[\frac{V_{t-2}^{x+1}-2V_{t-2}^x+V_{t-2}^{x-1}}{\triangle x^2}\right] + 4\gamma_{t-2}^x}{\triangle t^2} + \frac{-\omega\left[\frac{V_{t-3}^{x+1}-2V_{t-3}^x+V_{t-3}^{x-1}}{\triangle x^2}\right] - \gamma_{t-3}^x}{\triangle t^2} \tag{51}$$

Utilizing these approximations results in Equation 52.

$$
\begin{aligned}
a_1\ddot{I_C} + a_2\dot{I_C} + a_3 I_C \approx{}& \frac{2\omega a_1}{\triangle t^2 \triangle x^2}[V_t^{x+1} - 2V_t^x + V_t^{x-1}] + \frac{2a_1}{\triangle t^2}\gamma_t^x - ... \\
& \frac{5\omega a_1}{\triangle t^2 \triangle x^2}[V_{t-1}^{x+1} - 2V_{t-1}^x + V_{t-1}^{x-1}] - \frac{5a_1}{\triangle t^2}\gamma_{t-1}^x + ... \\
& \frac{4\omega a_1}{\triangle t^2 \triangle x^2}[V_{t-2}^{x+1} - 2V_{t-2}^x + V_{t-2}^{x-1}] + \frac{4a_1}{\triangle t^2}\gamma_{t-2}^x - ... \\
& \frac{\omega a_1}{\triangle t^2 \triangle x^2}[V_{t-3}^{x+1} - 2V_{t-3}^x + V_{t-3}^{x-1}] - \frac{a_1}{\triangle t^2}\gamma_{t-3}^x + ... \\
& \frac{3\omega a_2}{2\triangle t \triangle x^2}[V_t^{x+1} - 2V_t^x + V_t^{x-1}] + \frac{3a_2}{2\triangle t}\gamma_t^x - ... \\
& \frac{4\omega a_2}{2\triangle t \triangle x^2}[V_{t-1}^{x+1} - 2V_{t-1}^x + V_{t-1}^{x-1}] - \frac{4a_2}{2\triangle t}\gamma_{t-1}^x + ... \\
& \frac{\omega a_2}{2\triangle t \triangle x^2}[V_{t-2}^{x+1} - 2V_{t-2}^x + V_{t-2}^{x-1}] + \frac{a_2}{2\triangle t}\gamma_{t-2}^x + ... \\
& \frac{\omega a_3}{\triangle x^2}[V_t^{x+1} - 2V_t^x + V_t^{x-1}] + a_3\gamma_t^x
\end{aligned} \tag{52}
$$

New terms, α's and β's, are defined to keep the approximation orderly.

$$\alpha_1 = \frac{\omega a_1}{\triangle t^2 \triangle x^2} \tag{53}$$

$$\beta_1 = \frac{a_1}{\triangle t^2} \tag{54}$$

$$\alpha_2 = \frac{\omega a_2}{\triangle t \triangle x^2} \tag{55}$$

$$\beta_2 = \frac{a_2}{\triangle t} \tag{56}$$

$$\alpha_3 = \frac{\omega a_3}{\triangle x^2} \tag{57}$$

$$\beta_3 = a_3 \tag{58}$$

The coefficients are then grouped and the approximation rewritten in Equation 59.

$$
\begin{aligned}
a_1\ddot{I_C} + a_2\dot{I_C} + a_3 I_C \approx{}& V_t^{x+1}[2\alpha_1 + (3/2)\alpha_2 + \alpha_3] + V_t^x[-4\alpha_1 - 3\alpha_2 - 2\alpha_3] + ... \\
& V_t^{x-1}[2\alpha_1 + (3/2)\alpha_2 + \alpha_3] + V_{t-1}^{x+1}[-5\alpha_1 - 2\alpha_2] + V_{t-1}^x[10\alpha_1 + 4\alpha_2] + ... \\
& V_{t-1}^{x-1}[-5\alpha_1 - 2\alpha_2] + V_{t-2}^{x+1}[4\alpha_1 + (1/2)\alpha_2] + V_{t-2}^x[-8\alpha_1 - \alpha_2] + ... \\
& V_{t-2}^{x-1}[4\alpha_1 + (1/2)\alpha_2] + V_{t-3}^{x+1}[-\alpha_1] + V_{t-3}^x[2\alpha_1] + V_{t-3}^{x-1}[-\alpha_1] + ... \\
& \gamma_t^x[2\beta_1 + (3/2)\beta_2 + \beta_3] + \gamma_{t-1}^x[-5\beta_1 - 2\beta_2] + ... \\
& \gamma_{t-2}^x[4\beta_1 + (1/2)\beta_2] + \gamma_{t-3}^x[-\beta_1]
\end{aligned} \tag{59}
$$

The two approximations (Eq.'s 43 and 59) are assembled to form the complete finite difference approximation of the modified cable equation (Eq. 60).

$$V_t^{x+1}[-2\alpha_1-(3/2)\alpha_2-\alpha_3] + V_t^x[c_1+4\alpha_1+3\alpha_2+2\alpha_3] + V_t^{x-1}[-2\alpha_1-(3/2)\alpha_2-\alpha_3] =$$
$$V_{t-1}^{x+1}[-5\alpha_1 - 2\alpha_2] + V_{t-1}^x[-c_2 + 10\alpha_1 + 4\alpha_2] + V_{t-1}^{x-1}[-5\alpha_1 - 2\alpha_2]+$$
$$V_{t-2}^{x+1}[4\alpha_1 + (1/2)\alpha_2] + V_{t-2}^x[-c_3 - 8\alpha_1 - \alpha_2] + V_{t-2}^{x-1}[4\alpha_1 + (1/2)\alpha_2] + ...$$
$$V_{t-3}^{x+1}[-\alpha_1] + V_{t-3}^x[-c_4+2\alpha_1] + V_{t-3}^{x-1}[-\alpha_1] + V_{t-4}^x[-c_5] + ...$$
$$\gamma_t^x[2\beta_1+(3/2)\beta_2+\beta_3] + \gamma_{t-1}^x[-5\beta_1-2\beta_2] + \gamma_{t-2}^x[4\beta_1+(1/2)\beta_2] + ...$$
$$\gamma_{t-3}^x[-\beta_1] \tag{60}$$

Equation 60 is rewritten in matrix-vector form as shown below. In this form, it is apparent that the model can be described with four symmetric, tridiagonal matrices (A, B, C, and D) and several scalar terms. When simplified, this equation has the form Ax=b; the unknown, x, is the vector representing V_t^x and b is everything else, which is calculated as the system is solved. V_t^x is solved for with the tridiagonal matrix algorithm.

$$A\begin{bmatrix} V_t^1 \\ V_t^2 \\ V_t^3 \\ \vdots \\ V_t^n \end{bmatrix} = B\begin{bmatrix} V_{t-1}^1 \\ V_{t-1}^2 \\ V_{t-1}^3 \\ \vdots \\ V_{t-1}^n \end{bmatrix} + C\begin{bmatrix} V_{t-2}^1 \\ V_{t-2}^2 \\ V_{t-2}^3 \\ \vdots \\ V_{t-2}^n \end{bmatrix} + D\begin{bmatrix} V_{t-3}^1 \\ V_{t-3}^2 \\ V_{t-3}^3 \\ \vdots \\ V_{t-3}^n \end{bmatrix} - c_5\begin{bmatrix} V_{t-4}^1 \\ V_{t-4}^2 \\ V_{t-4}^3 \\ \vdots \\ V_{t-4}^n \end{bmatrix} + ...$$

$$\begin{bmatrix} \gamma_t^1 & \gamma_{t-1}^1 & \gamma_{t-2}^1 & \gamma_{t-3}^1 \\ \gamma_t^2 & \gamma_{t-1}^2 & \gamma_{t-2}^2 & \gamma_{t-3}^2 \\ \gamma_t^3 & \gamma_{t-1}^3 & \gamma_{t-2}^3 & \gamma_{t-3}^2 \\ \vdots & \vdots & \vdots & \\ \gamma_x^n & \gamma_{t-1}^n & \gamma_{t-2}^n & \gamma_{t-3}^n \end{bmatrix} \begin{bmatrix} 2\beta_1+\frac{3}{2}\beta_2+\beta_3 \\ -5\beta_1-2\beta_2 \\ 4\beta_1+\frac{1}{2}\beta_2 \\ -\beta_1 \end{bmatrix}$$

where,

$$A=\begin{bmatrix} c_1+2\alpha_1+\frac{3}{2}\alpha_2+\alpha_3 & -2\alpha_1-\frac{3}{2}\alpha_2-\alpha_3 & 0 & \dots & 0 \\ -2\alpha_1-\frac{3}{2}\alpha_2-\alpha_3 & c_1+4\alpha_1+3\alpha_2+2\alpha_3 & \ddots & \dots & \vdots \\ 0 & \ddots & \ddots & -2\alpha_1-\frac{3}{2}\alpha_2-\alpha_3 & 0 \\ \vdots & \dots & -2\alpha_1-\frac{3}{2}\alpha_2-\alpha_3 & c_1+4\alpha_1+3\alpha_2+2\alpha_3 & -2\alpha_1-\frac{3}{2}\alpha_2-\alpha_3 \\ 0 & \dots & 0 & -2\alpha_1-\frac{3}{2}\alpha_2-\alpha_3 & c_1+2\alpha_1+\frac{3}{2}\alpha_2+\alpha_3 \end{bmatrix}$$

$$B=\begin{bmatrix} -c_2+5\alpha_1+2\alpha_2 & -5\alpha_1-2\alpha_2 & 0 & \dots & 0 \\ -5\alpha_1-2\alpha_2 & -c_2+10\alpha_1+4\alpha_2 & \ddots & \dots & \vdots \\ 0 & \ddots & \ddots & -5\alpha_1-2\alpha_2 & 0 \\ \vdots & \dots & -5\alpha_1-2\alpha_2 & -c_2+10\alpha_1+4\alpha_2 & -5\alpha_1-2\alpha_2 \\ 0 & \dots & 0 & -5\alpha_1-2\alpha_2 & -c_2+5\alpha_1+2\alpha_2 \end{bmatrix}$$

$$C=\begin{bmatrix} -c_3-4\alpha_1-\frac{1}{2}\alpha_2 & 4\alpha_1+\frac{1}{2}\alpha_2 & 0 & \dots & 0 \\ 4\alpha_1+\frac{1}{2}\alpha_2 & -c_3-8\alpha_1-\alpha_2 & \ddots & \dots & \vdots \\ 0 & \ddots & \ddots & 4\alpha_1+\frac{1}{2}\alpha_2 & 0 \\ \vdots & \dots & 4\alpha_1+\frac{1}{2}\alpha_2 & -c_3-8\alpha_1-\alpha_2 & \\ 0 & \dots & 0 & 4\alpha_1+\frac{1}{2}\alpha_2 & -c_3-4\alpha_1-\frac{1}{2}\alpha_2 \end{bmatrix}$$

$$D=\begin{bmatrix} -c_4+\alpha_1 & -\alpha_1 & 0 & \dots & 0 \\ -\alpha_1 & -c_4+2\alpha_1 & \ddots & \dots & \vdots \\ 0 & \ddots & \ddots & -\alpha_1 & 0 \\ \vdots & \dots & -\alpha_1 & -c_4+2\alpha_1 & \\ 0 & \dots & 0 & -\alpha_1 & -c_4+\alpha_1 \end{bmatrix}$$

3.2.3.3 Determining γ

γ represents the effect of the ionic currents and the external, stimulating voltage on the cable model. It is a result of the previous derivations and defined in Equation 61.

$$\gamma_t^x = \frac{d}{4R_i}\frac{\partial^2 V_e}{\partial x^2} - I_{ion} \tag{61}$$

$\frac{\partial^2 V_e}{\partial x^2}$ is calculated using the activating function (Eq. 62), which is dependent on the

amplitude of the stimulating current (I_{stim}), the conductivity of the surrounding medium (σ_e), and the distance between the stimulus and the cable (h). Since all of these parameters are already known, $\frac{\partial^2 V_e}{\partial x^2}$ can be calculated for every point along the cable at every point in time prior to solving the system.

$$\frac{\partial^2 V_e}{\partial x^2} = \frac{I_{stim}}{4\pi\sigma_e}\left[\frac{2x^2 - h^2}{(h^2 + x^2)^{5/2}}\right] \tag{62}$$

The ionic current is the sum of the currents through the individual ion channels: sodium, potassium, and leakage (Eq. 63). The behavior of these ion channels is described by the Hodgkin-Huxley model (see the Background for further details). It relies on many different terms to describe the activation of the channels, including fixed ionic conductances, rate coefficients, and gating variables. The channel rate coefficients (Eq. 67 through 72) are voltage-dependent; they are calculated using the previous membrane voltage. ϕ represents the temperature-dependent component of the model; it is defined in Equation 73, where T is temperature in Celsius.

$$I_{ion} = I_{Na} + I_K + I_l \tag{63}$$

$$I_{Na}(V_m, t) = g_{Na}(V_m - E_{Na}), \tag{64}$$

$$I_K(V_m, t) = g_K(V_m - E_K), \tag{65}$$

$$I_l(V_m, t) = \bar{g}_l(V_m - E_l) \tag{66}$$

$$\alpha_n = \phi\frac{(0.1(1 - 0.1V))}{exp(1 - 0.1V) - 1} \tag{67}$$

$$\beta_n = \phi 0.125 exp\left(\frac{-V}{80}\right) \tag{68}$$

$$\alpha_m = \phi\frac{(2.5 - 0.1V)}{exp(2.5 - 0.1V) - 1} \tag{69}$$

$$\beta_m = \phi 4 exp\left(\frac{-V}{18}\right) \tag{70}$$

$$\alpha_h = \phi 0.07 exp\left(\frac{-V}{20}\right) \tag{71}$$

$$\beta_h = \phi\frac{1}{exp(3 - 0.1V) + 1} \tag{72}$$

$$\phi = 3^{(T-6.3)/10} \tag{73}$$

The rate coefficients are used to determine the status of the gating variables, which are described by first-order derivatives (Eq.'s 75, 77, and 78). The conductance of the ion channels are then determined by the gating variables (m, n, and h) and the conductance constants (g_K and g_{Na}).

$$g_K = \bar{g_K} n^4 \tag{74}$$

$$\frac{\partial n}{\partial t} = \alpha_n(1-n) - \beta_n n \tag{75}$$

$$g_{Na} = \bar{g_K} m^3 h \tag{76}$$

$$\frac{\partial m}{\partial t} = \alpha_m(1-m) - \beta_m m, \tag{77}$$

$$\frac{\partial h}{\partial t} = \alpha_h(1-h) - \beta_h h \tag{78}$$

The derivatives of m, n, and h are approximated using the backwards difference method, the results of which are described in Equations 79, 80, and 81. The new m, n, and h terms are calculated using their previous values.

$$m_{next} = \triangle t\alpha_m - (\triangle t\alpha_m + \triangle t\beta_m - 1)m_{prev} \tag{79}$$

$$n_{next} = \triangle t\alpha_n - (\triangle t\alpha_n + \triangle t\beta_n - 1)n_{prev} \tag{80}$$

$$h_{next} = \triangle t\alpha_h - (\triangle t\alpha_h + \triangle t\beta_h - 1)h_{prev} \tag{81}$$

The computation time of this model varies depending on the chosen parameters such as the fiber length, simulation duration, and step sizes, as well as the processing power of the computer. For the simulations performed in the results, the average time to compute the membrane voltage in space and time is around 15 minutes.

3.2.4 Solving the modified cable model

The modified cable model is implemented in C because it has less overhead than programs such as Matlab and it is the programming language I am most familiar with. Overhead is a significant consideration because of the long computation times involved in the execution of this model. The largest contributor to running time is the size of the temporal and spacial steps ($\triangle t$ and $\triangle x$). Smaller step sizes mean more points in time and space at which to perform calculations.

As discussed previously, solving the model is essentially solving the Ax=b system for the unknown x (the next membrane voltage). The matrix A is already known and b must be determined using the Hodgkin-Huxley equations and previous membrane voltages. The system is solved iteratively using two nested for loops. The first for loop steps through time, where, at each time point, the membrane voltage along the cable is calculated. The nested, second loop calculates the ionic current and effect of the external stimulus at each point long the cable, referred to previously as γ. The results of the γ calculations are part of the b component of Ax=b. Its previous two values are also needed, so they must be saved during the computation. The other components of b are the three previous values of the membrane voltage, attenuated by the matrices B and C and the scalar c_4.

Once b has been determined for the current time point, x is solved for using the tridiagonal matrix algorithm, which is applicable because A is a tridiagonal matrix. The temporal for loop progresses one time step and the previous membrane voltages will be used to calculate current one. The following list outlines the set of iterative calculations performed to solve the system for the membrane voltage.

1. Initialize model variables based on the system starting at rest
2. Calculate ion channel rate constants
3. Calculate gating variables
4. Calculate ion channel currents and sum for I_{ion}
5. Calculate γ from I_{ion} and external stimulus ($\frac{\partial^2 V_e}{\partial x^2}$)
6. Advance to the next space step and repeat from step 2 until the cable ends
7. Use the previous V_m values and new and previous γ values to calculate b, where b = BV^x_{t-1} + CV^x_{t-2} + DV^x_{t-3} - $c_5V^x_{t-4}$ + γ terms
8. Use the tridiagonal matrix algorithm to solve for the next V_m
9. Advance to the next time step and repeat from step 2 until the run time ends

CHAPTER IV

RESULTS

4.1 Unmodified cable model verification

The unmodified cable model is verified through comparison to papers implementing the cable model with extracellular stimulation. The first paper, *Analysis of Models for External Stimulation* by Rattay [14], examines the model behavior when stimulated with a rectangular cathodal impulse. Rattay plotted the threshold current needed to generate an action potential as a function of the axon diameter (d). It is apparent from this plot that as the diameter increases, the threshold current decreases. Figure 17 demonstrates that the results from my model are consistent in value and general trend with Rattay's results.

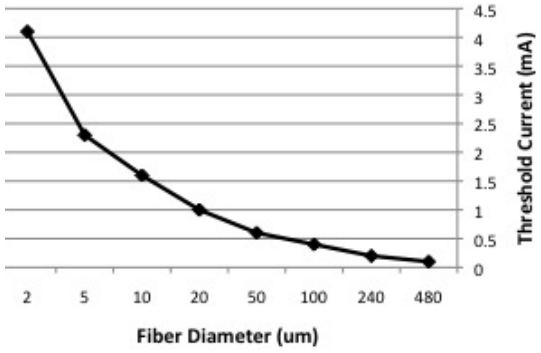

(a) Results from my cable model with external stimulation.

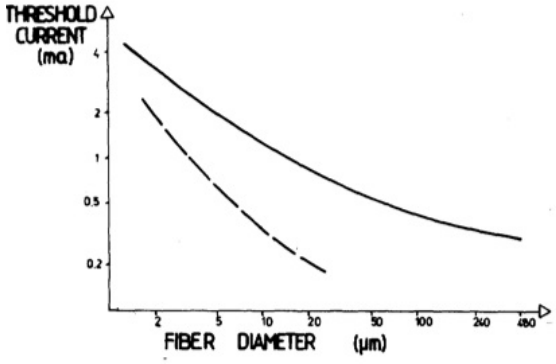

(b) Results from Rattay's cable model with external stimulation. The solid line is the one of interest.

Figure 17: Threshold current as a function of the fiber diameter. Stimulation occurs from a rectangular cathodal impulse of 0.1 ms, 1 mm away from the axon. The axon parameters used are those of squid nerve fiber.

In 1987, Rattay expanded on this model study by examining the relationship between stimulating current and distance between the stimulus and axon [15]. For a cathodal current, there exists a threshold at which impulse generation is achieved. As the current is increased, the area surrounding the active region becomes increasingly hyperpolarized by the stimulus, eventually blocking the impulse from propagating beyond it. An anodal stimulus will also

create a region of hyperpolarization that will block impulse propagation.

For a given stimulus current and fiber diameter (9.6μm), Rattay determined the range of distances between the electrode and fiber at which AP excitation would occur. He showed that, for a cathodal electrode current, there is an upper and lower bound of electrode position where AP generation will occur. If the electrode is too far away from the fiber, the effect on the membrane voltage will not be enough to trigger an AP. If the electrode is too close, the stimulus may depolarize the fiber around the electrode cite, therefore blocking AP generation and propagation. For anodal stimulation, the electrode cannot be too close to prevent AP excitation. Rattay's results from this experiment are plotted with the results from my model in Figure 18. There is some difference between Rattay's results and mine; this is due the the manner in which the AP excitation threshold is determined. The electrode stimulus is varied by a fixed amount until the excitation status changes, which means the threshold can fall within the step size used to augment the stimulus magnitude.

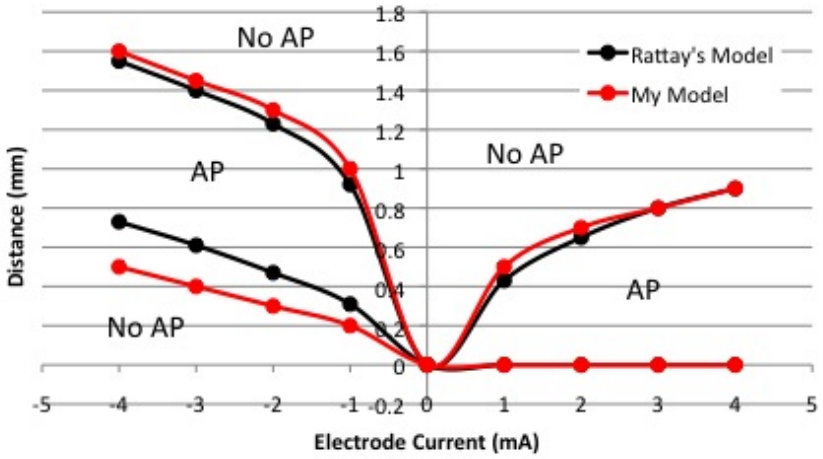

Figure 18: Plot of AP excitation as a function of electrode current and distance to the fiber. The model uses the squid axon properties and a fiber diameter of 9.6μm.

While Rattay focused only on impulse generation, Tai et al. [17] also examined impulse block in the cable model with extracellular stimulation. This model uses two external stimuli placed 0.1cm from the axon. A rectangular pulse is used for AP generation at 1cm and a 5kHz sinusoidal stimulus for block at 2.5 cm along a 4cm long fiber with a diameter of 10μm. The block stimulus is turned on first so that any impulses it initially

generates are not confused with the AP of interest generated by the current pulse. Given these parameters, Tai et al. show that the block current threshold lies between 12.2mA and 12.3mA. The block threshold refers to the current intensity at which conduction block first occurs. Using the same model parameters, my model results in a block threshold between 12.0mA and 12.1mA. Tai et al. also examined the relationship between axon diameter and block threshold at various HFAC stimulus frequencies.

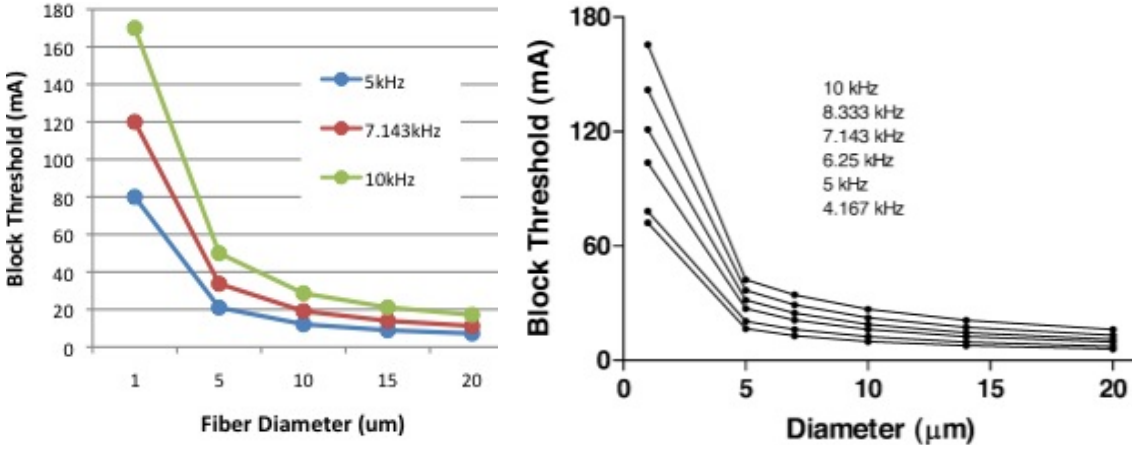

(a) Results from my cable model with external stimulation.

(b) Results from Tai et al. (2005) cable model with external stimulation.

Figure 19: Relationship between block current threshold and fiber diameter for various frequencies.

Figure 19 shows that the block threshold increases as a function of stimulus frequency and decreases as a function of diameter. Therefore, stimulation frequency can be varied to selectively block axons of different diameters.

To improve stability at smaller time steps and higher frequencies, the membrane voltage used to update the gating variables can be clipped to between -50 and 120mV (where 0mV is the resting potential). This is because the equations for the voltage-dependent time-constants decay towards zero at very high and low voltages. This is quite unrealistic, and an artifact of the membrane potential being well outside the range considered by Hodgkin and Huxley [9] when the model was developed. If the membrane voltage greatly exceeds the voltage range, as it does at the block site, then the gating variables will grow out of control. The clipping is solely used when updating the gating variables. To ensure that the clipping does not change the behavior of the cable model, the model is implemented with

and without clipping. As seen in Figure 20, clipping of the membrane voltage has very little effect on the relationship between block frequency and threshold.

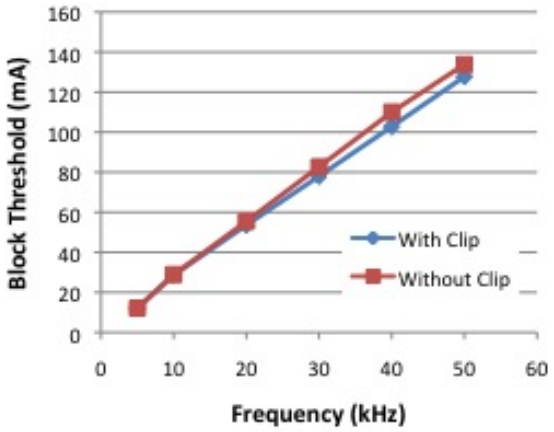

Figure 20: Relationship between block current threshold and frequency for the unmodified cable model with and without clipping. The model is implemented with the parameters used in the comparison to Tai's paper.

4.2 Modified cable model verification

The modified cable equation can be simplified to the unmodified cable equation by setting certain parameters, b_0, b_1, a_1, and a_2, to zero so that the relationship in Equation 82 simplifies to

$$b_2\dot{V_m} = a_3 I_C. \tag{82}$$

This expression says that the current through the membrane capacity is equal to a constant (b_2/a_3) times the derivative of the voltage across it; this is consistent with the current-voltage relationship of a capacitor if the constant is the capacity. Nullifying the before mentioned terms will cancel out the matrix D, the scalar c_5, and any previous terms of γ; it also modifies the matrices B and C and the coefficients of γ. What remains is consistent with the unmodified cable equation.

Figure 21 shows the membrane voltage and gating variables of the modified cable model without the FDC component at a point 1.75cm along the fiber, resulting from a 3mA current pulse with the block stimulus turned off. These values are plotted against the results of the unmodified cable model, which match very well.

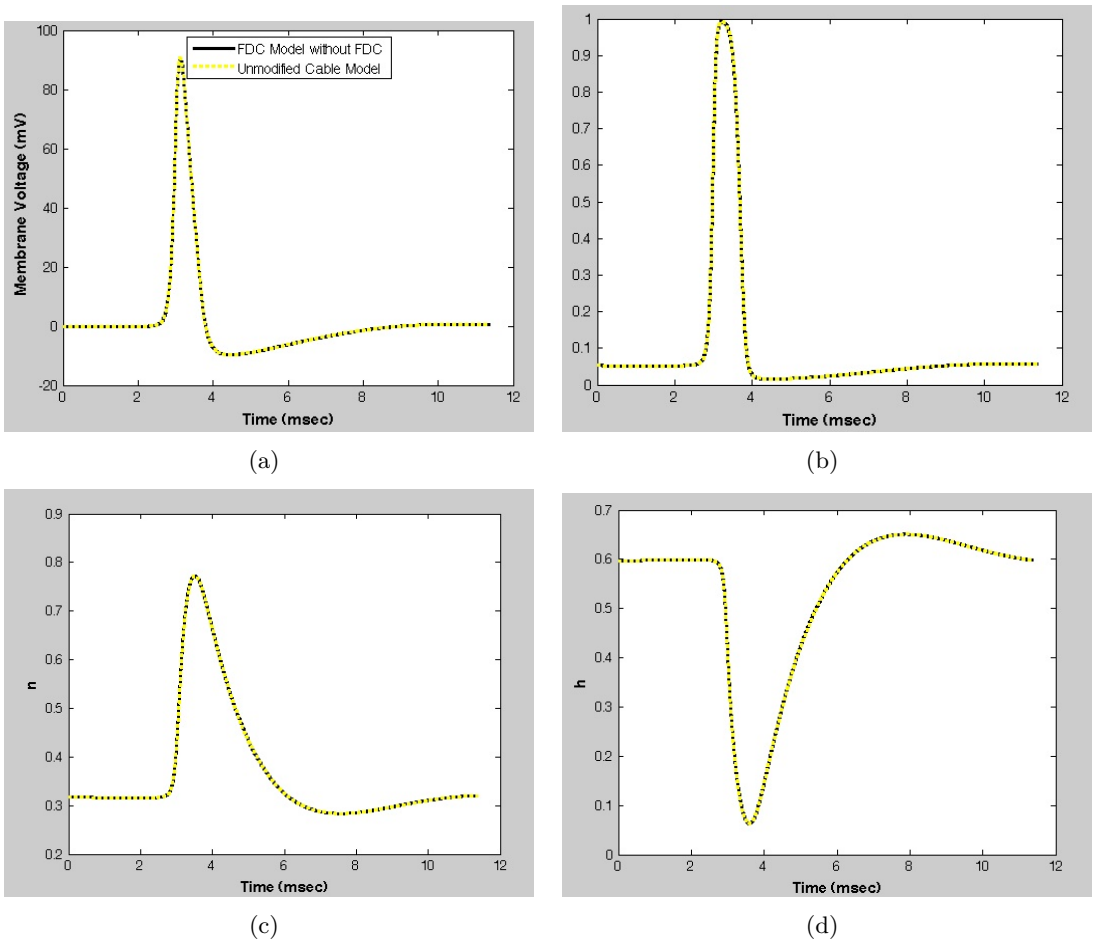

Figure 21: Modified cable model without the FDC component. Membrane voltage and gating variable values as an action potential propagates through a node 1.75cm along a cable with a 10μm diameter. The AP was generated by applying a -3mA current pulse at 0.1ms from the simulation start and no blocking stimulus.

In Figure 22, the modified cable model without FDC is compared to Tai (2005), as was done with the unmodified cable model in Figure 19. It is evident from these plots that the modified cable model without FDC is consistent with the unmodified cable model both in terms of the AP characteristics and the block threshold-frequency relationship. This comparison helps to ensure that the results of the FDC model are due to the addition of the FDC and not any changes in the computational methods or code.

Once the model has been implemented with the FDC component, it is necessary to verify that the model generates a propagating action potential. Figure 23 shows the membrane voltage and gating variables at a point 1.75cm along the fiber, resulting from a 3mA pulse

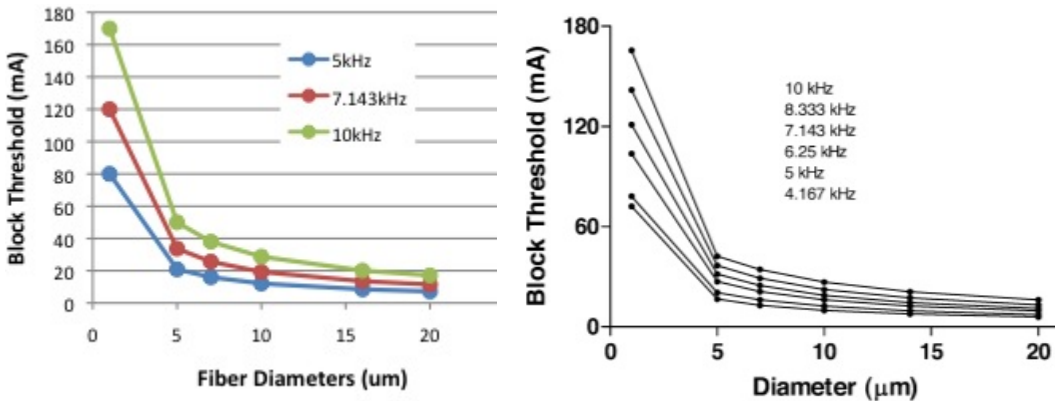

(a) Results from the FDC model without FDC. (b) Results from Tai et al. (2005) cable model.

Figure 22: Relationship between block threshold and fiber diameter for various frequencies.

at 0.1ms from the start with the block stimulus turned off. There is a difference in timing between the AP of the modified and unmodified cable model and a difference in the AP shape and duration.

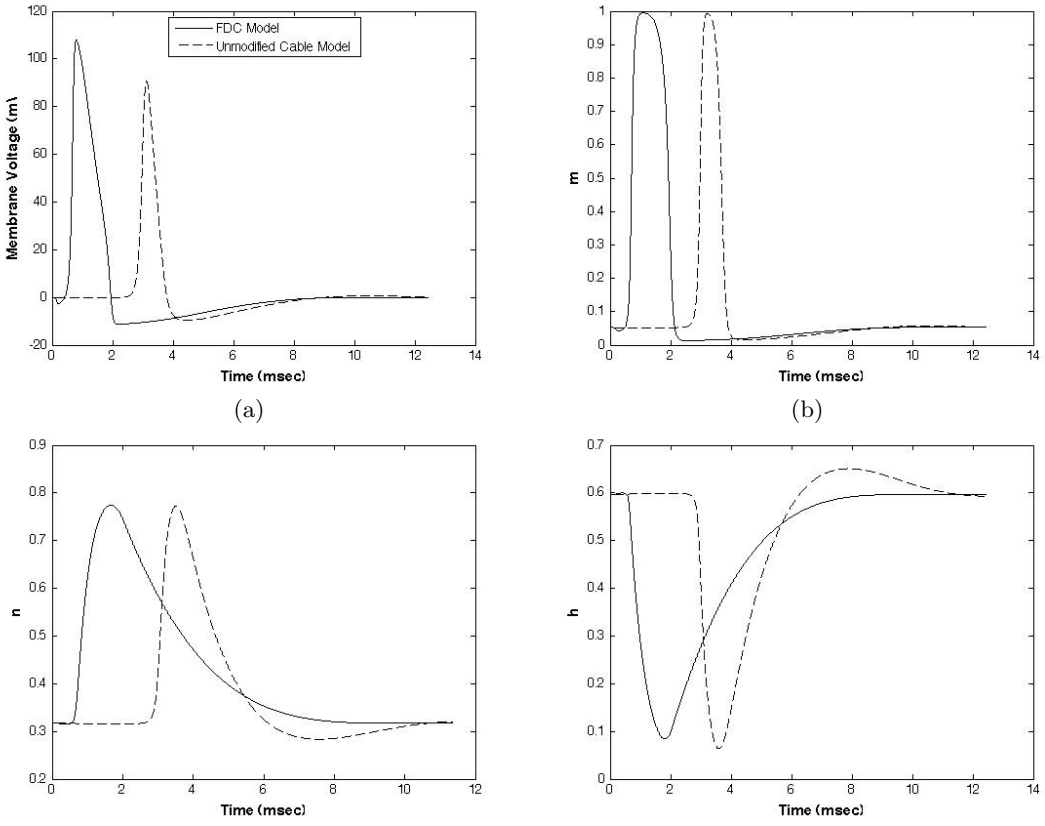

Figure 23: Membrane voltage and gating variable values as an action potential propagates through a node 1.75cm along a cable with a 10μm diameter.

The faster timing is caused by an increase in propagation velocity, which is likely an effect of modifying the membrane capacitance. The change in shape and duration of the AP and gating variables is also likely caused by the change in capacitance. However, the effect will require further investigation to be completely understood. Preliminary exploration of this effect has shown that varying the membrane capacitance in a single-node Hodgkin-Huxley model will result in a change in AP amplitude and duration (Figure 24).

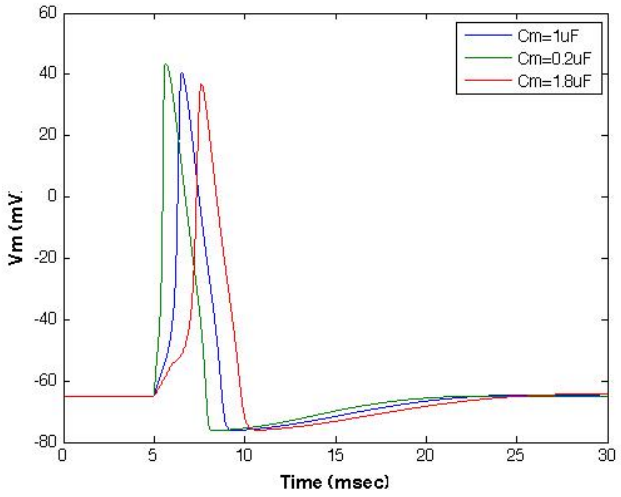

Figure 24: The membrane capacitance in varied in a Hodgkin-Huxley model (resting potential = -65mV) with a rectangular pulse stimulus of amplitude 20μA applied at 5ms.

The relationship between the block current threshold and frequency of the FDC model is plotted in Figure 25(b) against that of the unmodified cable model. The FDC model block threshold starts and remains low, near to the block threshold for the cable model at low frequencies. The variation in block threshold is so small that the relationship is practically flat. This response does not demonstrate the nonmonotonic response seen in animal experiments.

Besides methods of approximation, the choice in step size is extremely important. Clipping the membrane voltage for the gating variables will allow the model to compute at smaller time and space steps without incurring 'Not a Numbers' (NaNs), which result when the membrane voltage blows up. However, this doesn't guarantee that the model is stable at those time steps. To determine the minimum step sizes, the relationship between the block threshold and frequency of the modified cable model is plotted in Figure 26 for over

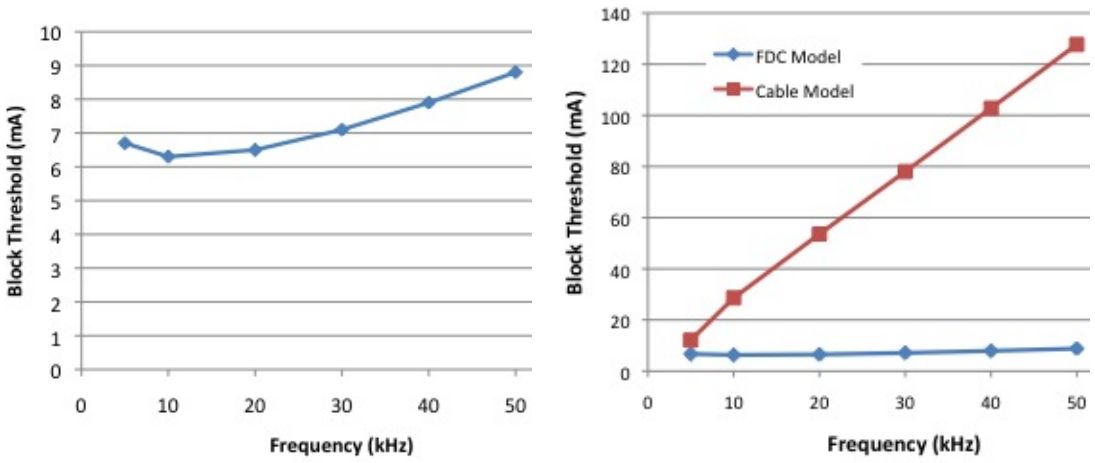

(a) Modified cable (FDC) model by itself. (b) Modified (FDC) and unmodified cable model.

Figure 25: Relationship between block current threshold and frequency for the modified (FDC) and unmodified cable model. Stimuli are 0.1cm away from an axon with diameter = 10um and length = 4cm.

a range of time steps (dt) and space steps (dx).

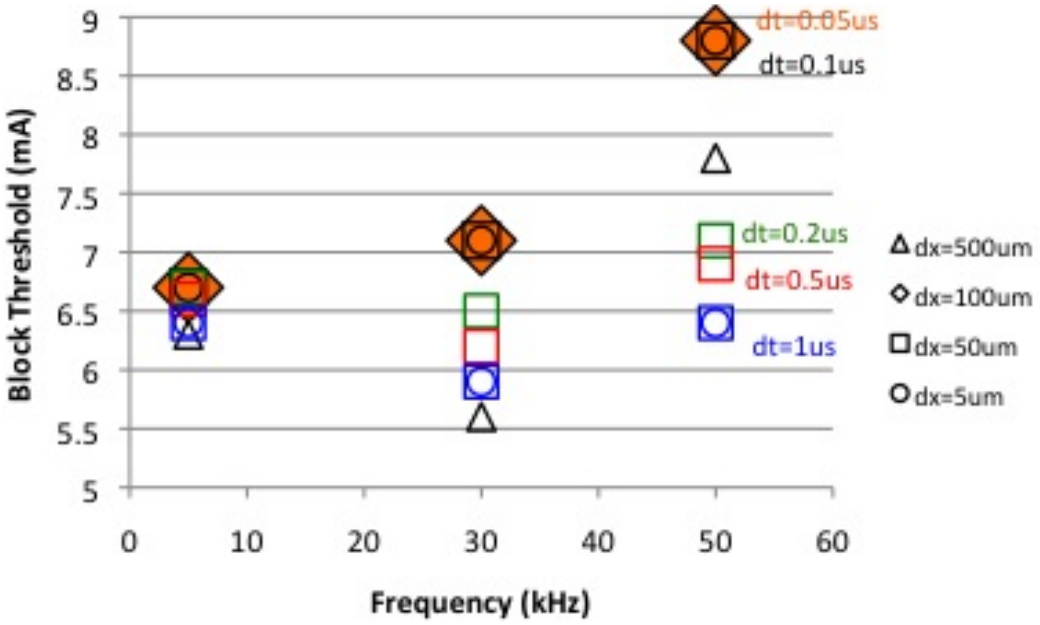

Figure 26: Relationship between block current threshold and frequency for the FDC model, as results from different time (dt) and space (dx) steps.

At large time steps the block threshold-frequency relationship is inconsistent, increasing as the step size decreases until 0.1μs. At this point the values converge and will remain the same even at smaller step sizes. Therefore, the minimum time step necessary to produce a

stable result is 0.1μs; Haeffele (2007) used time steps of 0.01μs. The space step (dx) results in stable calculations at 5μm, 50μm, and 100μm; at 500μm the model results become inconsistent.

CHAPTER V

CONCLUSION

This thesis has shown that it is possible to incorporate a frequency-dependent capacitance into the cable model in a way that is numerically stable. Through the use of finite difference approximations, the model is able to run at larger step sizes and is therefore more computationally efficient. This method also allows for the model to be formulated as an Ax=b problem, which is solved using the tridiagonal matrix algorithm. This formulation is more stable than the previous FDC model, where the model's PDE was approximated as a system of linear ODEs.

By adjusting certain parameter values, the modified cable model can be simplified to the unmodified cable model. A comparison of the block threshold-frequency relationship and AP shape prove that the modified cable model without the FDC component is consistent the fixed-capacitance cable model. When the FDC is reincorporated into the model, there is a difference in shape and time delay of the AP. Changing the membrane capacitance will cause a change in the propagation velocity and the amplitude and duration of the AP. However, further investigation is needed to fully understand the mechanisms behind this effect.

In the modified cable model, the relationship between the block threshold and frequency is significantly flattened compared to that of the cable model. The model response does not increase significantly with frequency and does not decrease at high frequencies, as was observed in animal studies. From this work, it seems unlikely that the FDC is the sole cause of the nonmonotonic blocking response of unmyelinated fibers.

REFERENCES

[1] Bahdra, N. and Kilgore, K., "Nerve conduction block utilizing high-frequency alternating current," Med. Biol. Eng. Comput., vol. 42, pp. 394–406, 2004.

[2] Bahdra, N. and Kilgore, K. L., "High-frequency electrical conduction block of mammalian peripheral motor nerve," Muscle Nerve, vol. 32, pp. 782–790, 2005.

[3] Bhadra, N., Bhadra, N., Kilgore, K., and Gustafson, K., "High-frequency electrical conduction block of the pudendal nerve," J Neural Eng., vol. 3, pp. 180–187, 2006.

[4] Bowman, B. R. and McNeal, D. R., "Response of single alpha-motoneurons to high-frequency pulse trains - firing behavior and conduction block phenomenon," Appl. Neurophysiol., vol. 49, pp. 121–138, 1986.

[5] Cattel, M. and Gerrard, R. W., "Action potentials during high and low frequency stimulation of medullated nerve," Science, vol. 28, pp. 645–646, 1935.

[6] Conte, S. and deBoor, C., Elementary Numerical Analysis. New York: McGraw-Hill, 1972.

[7] Haeffele, B. and Butera, R. J., "Modifying the hodgkin-huxley model for high frequency stimulation," Proc. 3rd Int. IEEE/EMBS Conf. on Neural Eng., pp. 550–552, 2007.

[8] Haydon, D. A. and Urban, B. W., "The admittance of the squid giant axon at radio frequencies and its relation to membrane structure," J. Physiol., vol. 360, pp. 275–291, 1985.

[9] Hodgkin, A. L. and Huxley, A. F., "A quantitative description of membrane current and its application to conduction and excitation in nerves," J Physiol, vol. 117, no. 4, p. 500544, 1952.

[10] Joseph, L. and Butera, R. J., "Conduction block in unmyelinated nerves using high frequency ac stimulation," Proc. 3rd Int. IEEE/EMBS Conf. Neural Eng., pp. 575–577, 2007.

[11] Joseph, L. and Butera, R. J., "Unmyelinated aplysia nerves exhibit a monotonic blocking response to high-frequency stimulation," IEEE Trans. Neural Systems and Rehabilitation Eng., vol. 17, no. 6, pp. 537–544, 2009.

[12] Joseph, L. and Butera, R. J., "High frequency stimulation selectively blocks different types of sciatic nerves," in review, 2011.

[13] McNeal, D. R., "Analysis of a model for excitation of myelinated fiber," IEEE Trans. Biomed. Eng., vol. 23, pp. 329–337, 1976.

[14] Rattay, F., "High frequency electrostimulation of excitable cells," J. Theor. Biol., vol. 123, pp. 45–54, 1986.

[15] Rattay, F., "Ways to approximate current-distance relations for electrically stimulated fibers," J. Theor. Biol., vol. 125, pp. 339–349, 1987.

[16] Reboul, J. and Rosenblueth, A., "The action of alternating currents upon the electrical excitability of nerve," American Journal of Physiology, vol. 125, no. 2, pp. 205–215, 1939.

[17] Tai, C., de Groat, W. C., and Roppolo, J. R., "Simulation of nerve block by high-frequency sinusoidal electrical current based on the hodgkin-huxley model," IEEE Trans. on Neural Sys. and Rehab. Eng., vol. 13, no. 7, pp. 415–421, 2005.

[18] Tanner, J. A., "Reversible blocking of nerve conduction by alternating-current excitation," Nature, vol. 195, pp. 712–713, 1962.

[19] Woo, M. Y. and Campbell, B., "Asynchronous firing and block of peripheral nerve conduction by 20 kc alternating current," Bull Los Angel Neuro Soc., vol. 29, pp. 87–94, 1964.